NASA Contractor Report 181670

A MICROMECHANICS MODEL OF THE STIFFNESS AND STRENGTH OF LAMINATES WITH FIBER WAVINESS

Charles E. Harris and Jong-Won Lee
Texas A&M University
College Station, Texas

NAG1-711
July 1988

National Aeronautics and
Space Administration

Langley Research Center
Hampton, Virginia 23665-5225

TABLE OF CONTENTS

LIST OF FIGURES

LIST OF TABLES

LIST OF SYMBOLS

C_i - unknown constants to be determined by the Rayleigh-Ritz method

D - flexural rigidity of a beam

E, E_f - Young's modulus of the wavy layer or fiber

E_m, E_T, E_t, E_r - Young's modulus of the matrix material

F - P

f - frequency of the moire grating

G_f - shear modulus of the fiber

G_m, G_{XZ} - shear modulus of the matrix material

H_o - max. rise of the initial wavy pattern

h_1 - half thickness of the wavy layer or fiber

h_2 - half thickness of one representing segment

I - moment of inertia of the main load carrying layer or fiber

K_L - linear spring constant of the matrix material

K_l - linear spring constant of the lower matrix material

K_u - linear spring constant of the upper matrix material

K_T - torsional spring constant of the matrix material

k - spring constant

L - half pitch of the wavy pattern

l_u - thickness of the matrix material above the wavy layer

l_l - thickness of the matrix material below the wavy layer

M - moment

P, P_1 - far-field load on the wavy layer or fiber

P_{cr} - critical load for buckling

S - total length of the neutral axis before deformation

t_r - thickness of the resin-rich region

v_f - fiber volume fraction

w_o - Z_o

w, w_2 - Z_1

x - axis representing the fiber direction

Z - through-the-thickness direction

Z_o - initial amplitude of the wavy layer

Z_1 - change of the wavy pattern in the Z axis

α - correction factor

Δ - rigid body displacement due to straightening of the wavy layer

ΔN_x - the increment of number of fringes in the axial(x) direction

ΔN_y - the increment of number of fringes in the transverse(Z) direction

$\Delta T/\Delta x$ - torque per infinitesimal length in the x axis direction

ΔU_x - displacement in the axial(x) direction

ΔU_y - displacement in the transverse(Z) direction

ϵ_o - far-field strain in the x axis direction

ϵ_{cr} - critical far-field strain for tension failure or yield

ϵ_{diff} - the average difference in the bending strain component between the upper and lower surfaces of the wavy layer

ϵ_{IND} - measurable strain

ϵ_{PS} - pseudo strain

ϵ_{xx} - actual value of the axial strain in a wavy layer

ϵ_{YLD} - yield strain of the wavy layer

θ_o - initial angle of the fiber with respect to the x axis

θ_f - dZ_1/dx

θ_m - angular deformation of the matrix material

Π = total potential energy

σ_f = far-field stress of the fiber

σ_{cr} = critical far-field stress for buckling

ν_m = Poisson's ratio of the matrix material

INTRODUCTION

The behavior of fiber-reinforced composite materials containing wrinkled fibers or wavy patterns in the main load-carrying layers has been the subject of considerable interest. Fibers or the main load-carrying layers may become wavy during manufacturing procedures such as filament winding, braiding, and stitching used to achieve through-the-thickness reinforcing. Furthermore, local geometric imperfections may develop as a result of twisted fiber bundles, air pockets, or the excess resin in local resin-rich regions. A number of experimental investigations[1-6] have shown that laminates with these wrinkled fibers, wavy layers or local geometric imperfections do not develop their full strength or stiffness under tensile or compressive loading. While geometric imperfections have been the subject of a number of rather specific analytical investigations, there does not exist a relatively simple micromechanics based model for the design or analysis of a general laminate with local curvature under either tension or compression loading. The development of a simple mathematical model for predicting the effective laminate strength and stiffness and the associated experimental confirmation of the theoretical assumptions and model results is the objective of the research described herein.

A simple mathematical model describing the deformation behavior of the main load-carrying layer of a laminated composite is developed herein. The main load-carrying layers, or the principal load-carrying layers, have initial curvature and are modelled as curved beams sup-

ported by a continuous elastic foundation. The stiffness of the elastic foundation represents the constraint on the main load-carrying layer provided by the filler material. Model formulations include the geometry where the layers are exactly In-Phase or parallel and where the layers are Out-of-Phase. The deformation behavior of the filler material for these two extreme cases is different and, therefore, necessitate a different formulation of the elastic foundation "spring" constants. The principle of minimum potential energy is used to develop the governing equations and the accuracy of the analytical results are examined by a carefully planned experimental program. Finally, the usefulness of the mathematical models is examined by several applications to "real" composites with in-situ local curvature. Model results are compared to available experimental results from the open literature.

Following the literature survey, the theoretical development is presented along with analytical parameter sensitivity studies. The experimental program is then described and experimental results are compared to the analytical results. The final chapter presents a discussion of the application of the model to real composites and concludes with a comparison of model predictions to available experimental results for real composites.

PROBLEM BACKGROUND

The problem background is discussed by way of the literature review presented in this section. The presentation of the literature is divided into two topics. The first topic addresses the engineering and research studies that have explored the effects of local curvature on the stiffness and strength of laminated composites and a metal matrix composite[1-6]. This work provides the motivation for the subject research. The second topic describes those studies that have developed an analytical treatment of the local curvature problem[7-14]. This discussion will establish the state-of-the-art of the design methodology when local curvature is present in laminated composites.

PREVIOUS EXPERIMENTAL STUDIES

Poe, et al.[1] conducted a test program to determine the residual tensile strength of a thick filament-wound solid rocket motor case after low-velocity impacts. They reported that the undamaged strength of specimens cut from a filament-wound case reinforced by unidirectional layers was 39% less than the expected strength on the basis of fiber-lot-acceptance tests. It was observed that the main load-carrying layers became wavy during manufacturing. A specimen edge cut from the filament wound graphite epoxy cylinder contains many wavy patterns in the main load-carrying layers, actually 0 degree layers, as shown in Fig. 1.

An experimental study of stitched composite laminates conducted by Dexter and Funk[2] showed a similar result. Their experimental result shows that the tensile and compressive strength of stitched laminates

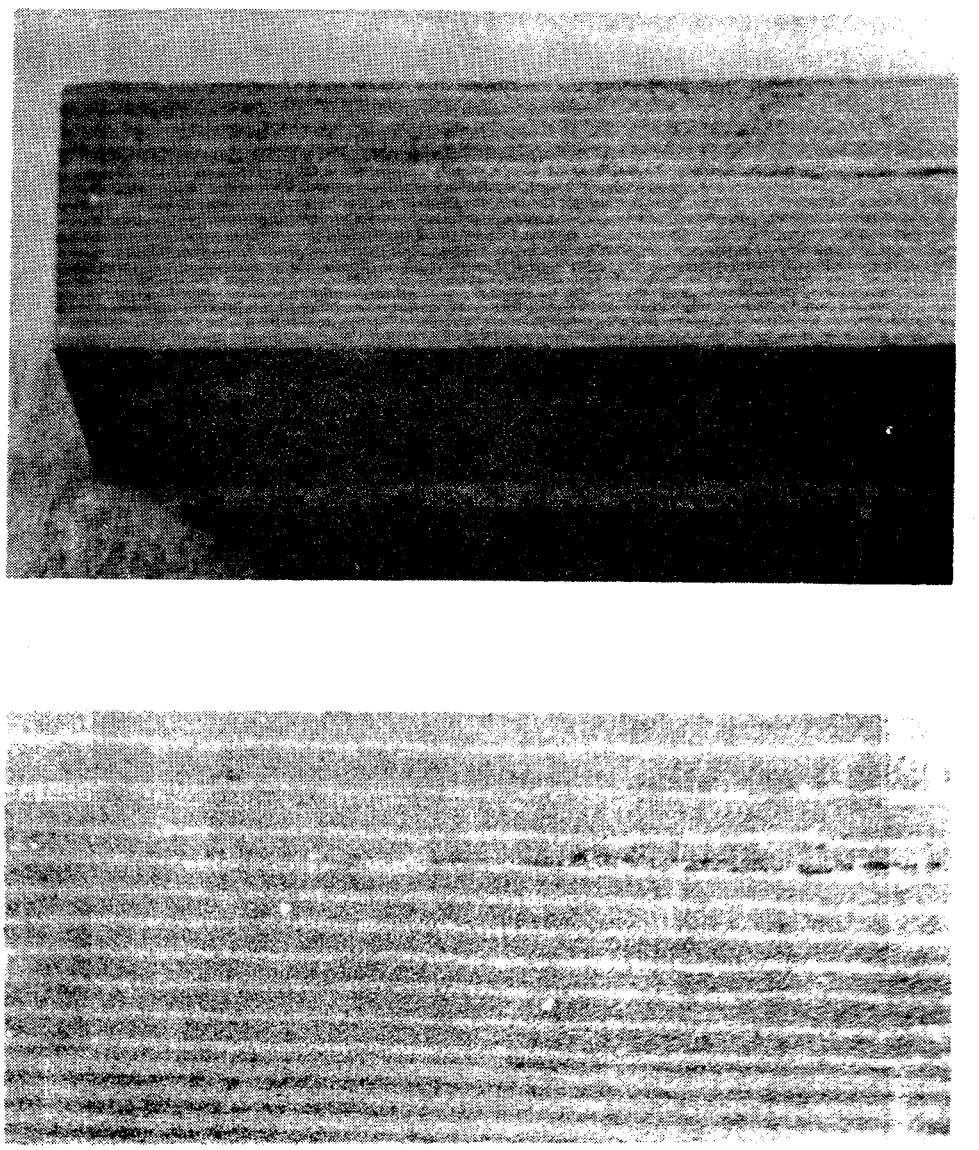

Fig. 1 Wavy Patterns in 0^{o} Reinforcing Layers in a Filament Wound Composite Specimen[1].

was approximately 20-25 % lower than the strength of unstitched laminates. Furthermore, the tensile strength of the stitched laminates decreased as the number of stitches increased, while the compressive strength increased.

Kagawa, et al.[3] obtained a larger ultimate tensile strain at small expense of the ultimate stress using helical fibers instead of straight fibers in a tungsten-copper metal matrix composite. They reported that the tensile fracture behavior of the helical fiber composite was not so catastrophic as that of the straight fiber composite, and suggested that tougher composite materials could be available using helical fibers instead of straight fibers in the metal matrix composite. In Fig. 2, the helical fibers surrounded by a copper matrix are shown with one possible combination of the hybrid wavy pattern, i.e., one In-Phase and one Out-of-Phase wavy pattern.

Makarov and Nikolaev[4] investigated the effect of curvature of the reinforcing fibers on the mechanical properties of composites through an experimental study using a low modulus matrix and high modulus reinforcing fibers. They concluded that the initial curvature of the reinforcing fibers must be taken into consideration in calculating the effective Young's modulus in the fiber direction.

Simonds, et al.[5] reported that the tensile strength of the AS4-3501 braided composite material of which the braid angle was 12^{o}-15^{o} was 30 to 50 % greater than the tensile strength of 15^{o} angle-ply laminates made of AS1-3501 graphite/epoxy. In addition the Young's modulus measured in the 0^{o} direction was almost the same as that of the 15^{o} angle-ply graphite/epoxy laminate.

Davis[6] presented results of an experimental investigation of the

(a)

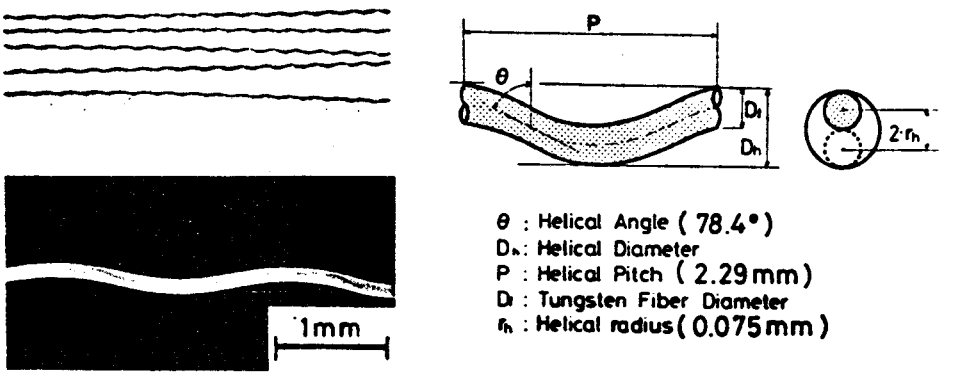

(b)

Fig. 2 Copper Matrix Metal Composite[3]

(a) Helical Tungsten Fiber
(b) Hybrid Wavy Pattern of Tungsten Fiber in Copper Matrix

compressive strength of unidirectional boron/epoxy composite materials with initially curved fibers. He obtained experimental evidence that showed that the shear modulus was related to the axial compressive stress.

It is obvious from these experimental investigations that local ply or local fiber curvature can result in significant differences in the stiffness and strength of otherwise straight laminated composites. Therefore, a proper design of a composite with local curvature in the reinforcement would require a mathematical model that accurately predicts the local and global deformation behavior of the composite.

PREVIOUS MODELS

The analysis of compressively loaded laminated composites with local fiber or layer curvature has been the subject of a number of investigations. In several cases, simple micromechanics based models of compressive strength have been formulated. The work of Rosen[7] is considered to be classical for predicting the compressive strength of a composite material with straight fibers as the reinforcement.

Rosen developed two analytical models for predicting the compressive strength of a fiber reinforced composite[7] by assuming the fibers as plates imbedded in a homogeneous matrix material. By applying the energy method to two extreme cases of fiber buckling, i.e., the extension mode and the shear mode, he derived compact analytical solutions to the critical stress and strain of straight fibers surrounded by matrix material which was relatively less stiff than the fibers.

However, mathematical modeling for the tension problem is still in

its infancy[8-13]. There is no counterpart to Rosen's compressive strength model for the tensile loading case. The tie-bar/column approach of Bert[8] may be the most likely candidate model for solving the tension problem of wrinkled fibers or wavy layers. But his governing differential equation is not directly applicable to a laminated composite, because it was derived for a rigid fiber imbedded in an infinite matrix material.

Bert[8] reviewed a number of mathematical models and proposed two methods: the mean-fiber-angle approach; and the elastically supported tie-bar/column approach, to explain the differences in tension and compression behavior of fiber-reinforced composites with locally curved fibers. He concluded that a definitive experimental program is required to determine which of the two methods is most efficient to predict the mechanical behavior of composites containing wavy patterns. Also, he emphasized the development of an experimental program to determine the role of interfacial adhesion between the fibers and matrix on the global behavior of composite materials with wavy patterns.

Jortner[9] constructed a theoretical model from which all elastic constants and thermal coefficients of a composite containing In-Phase wrinkled fibers can be estimated. After implementing his method by numerically satisfying stress equilibrium and strain compatibility simultaneously, he recommended comparing his model predictions to experimental data or with other finite-element models.

Akbarov and Guz[10,11] developed two mathematical models based on the linear elasticity theory and piecewise homogeneity to determine the stress-strain state of laminated composites containing wavy layers under a remote uniform tensile loading. From their model, the interfa-

cial stress components between the main load-carrying layers and filler layers can be predicted numerically. They calculated two interfacial stress components, which are normal and tangential to the interface between the matrix material and a curved layer, by satisfying the equations of equilibrium, Hooke's law, and the Cauchy relationships. In ref.[10], they assumed a very thick matrix layer and neglected the mutual influence between wavy layers. In ref.[11], they extended the approach proposed in ref.[10] including the mutual influence of adjacent wavy layers. In both studies, they found that a small-scale curvature gave a significant effect on the stress-strain state in a composite. However, as Akbarov and Guz mentioned in their papers, it is very cumbersome to compare any experimental data to their models because of the complexity of the mathematical formulations.

Ishikawa, et al.[12] also proposed two models, the mosaic and fiber undulation models, for predicting the effective elastic moduli of fabric composites. Their experimental results showed that the ratio of ply thickness to thread width, i.e. pitch of the wavy pattern, was a very important parameter which had a significant effect on the elastic moduli of plain weave composites.

El-Senussi and Webber[13] presented a theoretical analysis for the crack propagation of a layered strip in compression, in the presence of a blister. They proposed a typical set of design curves which showed the influence of blister length, applied strain and resin stiffness on loads required for splitting the reinforcing layer from the blister. Their approach for determining the deformed shape of the layered strip on the blister was exactly the same as the tie-bar/column approach proposed by Bert[8], except for the inclusion of the equivalent spring

constant for the elastic constraint due to the blister.

Shuart[14] investigated the short-wavelength buckling(or the micro-buckling) and the interlaminar and inplane shear failures of multi-directional composite laminates under uniaxial compression. He assumed the fibers in the lamina as a plate, and the matrix in the lamina as an elastic foundation. After his numerical analysis, he recommended additional experimental verification of his detailed 3-D analysis. (Reference 14 also contains a complete literature review of the compression loading problem and a genesis of the fiber buckling and compressive strength models.)

All of these theoretical studies have shown that relatively small-scale wavy patterns or wrinkles produce a noticeable effect on the stress-strain behavior of the composite material system. However, difficulties arise when we try to directly compare the experimental data published in the literature with those theories. This is because most of the mathematical models mentioned above are too complicated to apply directly. Among those mathematical models, the tie-bar/column approach proposed by Bert[8] and Rosen's model[7] are relatively simple. However, Rosen's model requires modification for solving the tension problem, and Bert's model needs more verification of its governing differential equation and elastic constraint due to the matrix layer. Therefore, the author has developed a new and simple deformation based mathematical model which includes geometrical parameters as well as material parameters for predicting stress-strain behavior of wavy laminates under tension loading.

MATHEMATICAL MODEL

The theoretical development of a mathematical model of the local deformation and state of strain of a wavy layer or a wrinkled fiber in a laminated composite proceeds from the micromechanics viewpoint. Concepts of strength-of-materials are applied to a representative segment of a single wavy layer. The geometry of the model is shown in Fig. 3. The In-Phase layer (Fig. 3a) and the Out-of-Phase layer (Fig. 3b) are treated as the two extreme cases. A single wavy layer is analyzed as a corrugated beam on an elastic foundation(Fig. 3c), where the stiffness of the elastic foundation represents the kinematic constraint on the wavy layer from the surrounding filler material.

The tension-compression behavior of the filler material is modeled as an array of linear springs, and the shear deformation behavior is modeled as an array of torsional springs. Since the curvature of the wavy layer is small relative to the length of the segment(pitch), the Euler-Bernoulli beam theory is applied. The governing differential equation for the initially curved beam on an elastic foundation is developed from the principle of minimum potential energy. Using the Cartesian coordinate system shown in Fig. 3c, the total potential energy of the beam is given by

$$\Pi = \frac{1}{2}\int_0^L \left\{ P\epsilon_o + EI\left[\frac{d^2 Z_1}{d\,x^2}\right]^2 + K_L(Z_1)^2 + K_T\theta_m{}^2 \right\} dx \qquad (1)$$

$$- P\,(\,\Delta + PL/2h_1E\,)$$

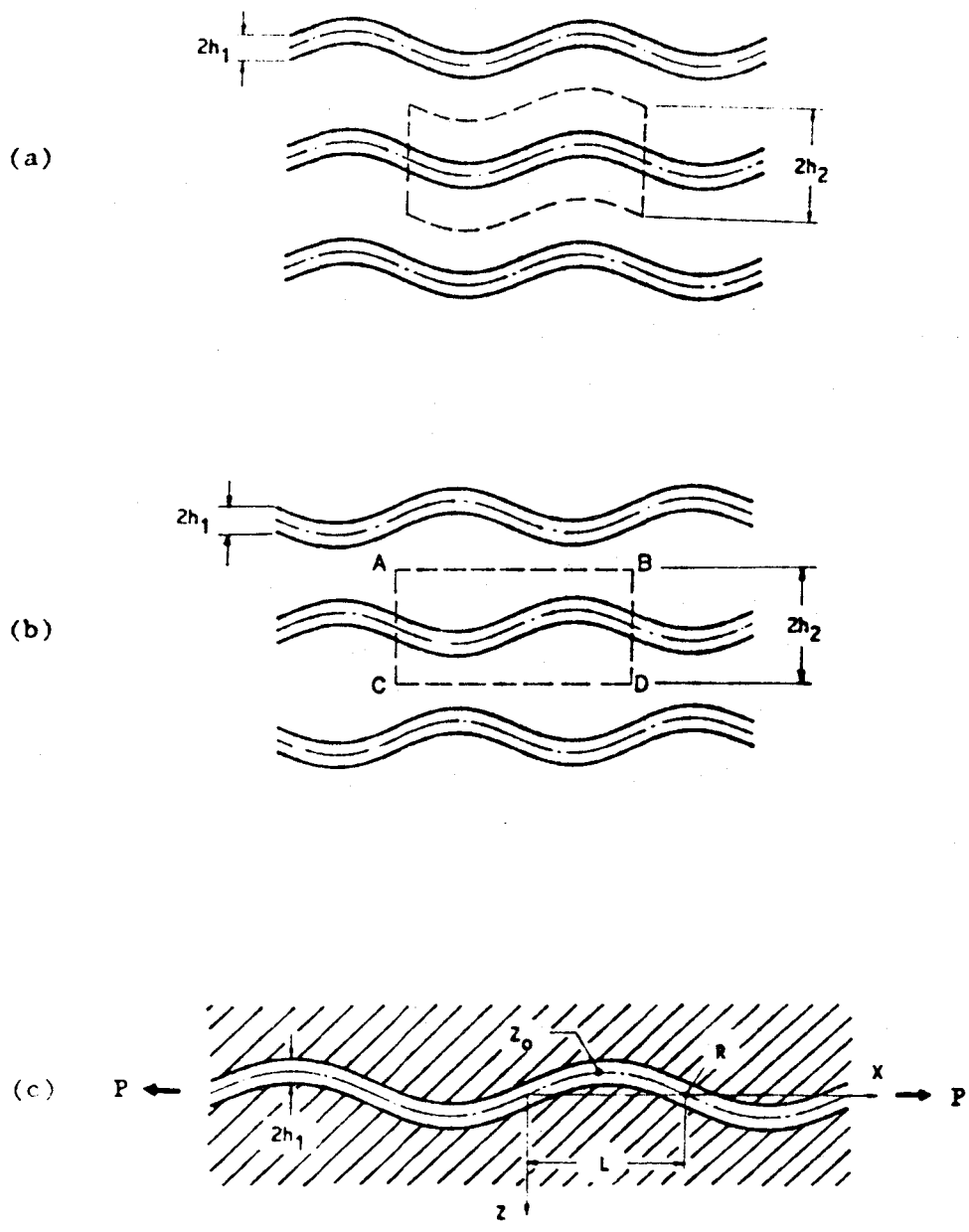

Fig. 3 Wavy Layers

(a) In-Phase
(b) Out-of-Phase
(c) General Case

where

EI = flexural rigidity of the wavy layer/unit width

K_T = torsional spring constant of the matrix material/unit width

K_L = linear spring constant of the matrix material/unit width

Z_1 = transverse displacement of the mid-surface of the wavy layer

Z_o = initial amplitude of the wavy layer

P = far field axial load on the wavy layer/unit width

ϵ_o = far-field axial strain

Δ = pitch increase due to straightening of the wavy layer

θ_m = angular deformation of the matrix

$= \alpha \, dZ_1/dx$

α = a constant calculated from the matrix deformation kinematics

The horizontal displacement (Δ) of point R in Fig. 3c, which causes pseudo strain can be calculated under the assumption that the neutral axis is incompressible, in other words the total length of the neutral axis, S, is assumed to remain constant[18]. Therefore,

$$S = \int_0^L \sqrt{1 + (dZ_o/dx)^2}\, dx$$

$$= \int_0^{L+\Delta} \sqrt{1 + [d(Z_1+Z_o)/dx]^2}\, dx \qquad (2)$$

Expanding in a binomial series and neglecting higher order terms, the horizontal displacement of point R due to the initial curvature is given by

$$\Delta = \frac{1}{2}\int_0^L \{ (dZ_o/dx)^2 - [d(Z_o+Z_1)/dx]^2 \} dx \qquad (3)$$

The axial strain of the neutral axis due to tension is assumed to be constant.

$$\epsilon_o = P/2h_1E \qquad (4)$$

The assumed boundary conditions are

$$Z_1 = \frac{d^2Z_1}{d\,x^2} = 0 \quad \text{at} \quad x = 0 \text{ and } L \qquad (5)$$

(Note that fixed end boundary conditions may also be assumed.)

The equilibrium deformation configuration of the modeled geometry corresponds to the stationary values of the total potential energy. These values are obtained by setting the variation of Π equal to zero. Therefore, the governing equation is obtained as follows:

$\delta\Pi = 0$, or

$$0 = \int_0^L (EIZ_1"\delta Z_1"+K_LZ_1\delta Z_1+\alpha^2K_TZ_1'\delta Z_1'+P(Z_o-Z_1)'\delta Z_1')dx \qquad (6)$$

where $Z_1'' = d^2Z_1/dx^2$

and $Z_1' = dZ_1/dx$.

Integrating eq. (6) by parts and substituting eqs. (3), (4) and (5), we obtain the following governing differential equation.

$$EI\frac{d^4Z_1}{dx^4} - (\alpha^2K_T+P)\frac{d^2Z_1}{dx^2} - \alpha^2\frac{dK_T}{dx}\frac{dZ_1}{dx} + K_L(x)Z_1 = P\frac{d^2Z_o}{dx^2} \tag{7}$$

For a single layer without matrix or an In-Phase wavy layer, the solution of this governing equation is easily obtained. Since it is very cumbersome to obtain an exact analytical solution for an Out-of-Phase wavy layer, the Rayleigh-Ritz method is appropriate to calculate an approximate solution. Since the general solutions of the transverse displacement, Z_1, are determined as a function of the applied far-field load P, the axial strain at any location of the wavy layer is given by

$$\epsilon_{xx} = \frac{P}{2Eh_1} - Z\frac{d^2Z_1}{dx^2}, \quad -h_1 \le Z \le h_1 \tag{8}$$

The pseudo-strain, i. e. the apparent strain at an arbitrary point along the wavy layer due to the rigid body motion associated with straightening the wavy layer, is given by

$$\epsilon_{PS}(x) = -\frac{1}{2}\left\{ \left[\frac{dZ_o}{dx}\right]^2 - \left[\frac{d(Z_o+Z_1)}{dx}\right]^2 \right\} \tag{9-a}$$

The average pseudo-strain along the one representing pitch of the wavy pattern is given by

$$\epsilon_{PS,AVE} = \frac{1}{2L}\int_0^L \left\{ \left[\frac{dZ_o}{dx}\right]^2 - \left[\frac{d(Z_o+Z_1)}{dx}\right]^2 \right\} dx \qquad (9\text{-b})$$

The indicated strain, i. e. the observed apparent strain which is the sum of the actual strain in the wavy layer and the pseudo-strain, can be predicted by

$$\epsilon_{IND}(x) = \epsilon_{xx} + \epsilon_{PS}(x) \qquad (10\text{-a})$$

$$\epsilon_{IND,AVE} = \epsilon_o + \epsilon_{PS,AVE} \qquad (10\text{-a})$$

A maximum strain failure criterion may then be applied to determine the far field strain at which failure of the wavy layer occurs. The maximum strain failure criterion can be written as

$$(\epsilon_{xx})_{MAX} = [\epsilon_{IND}(x) - \epsilon_{PS}(x)]_{MAX} \leq \epsilon_{YLD} \qquad (11)$$

where the tensile yield strain, ϵ_{YLD}, corresponds to the tensile yield or ultimate strain of a straight layer of the same material.

Specialized forms of the governing differential equation and the solutions for a single corrugated beam, In-Phase wavy layers, and Out-of-Phase wavy layers are developed in the following sections.

SINGLE CORRUGATED BEAM

Let the positive direction of the moment due to the axial force, P, be counterclockwise in Fig. 4. Then from the moment equilibrium,

$$\Sigma M = EI\frac{d^2Z_1}{dx^2} - PZ_o - PZ_1 = 0 \tag{12}$$

Rearranging gives

$$\frac{d^2Z_1}{dx^2} - \frac{PZ_1}{EI} = \frac{PZ_o}{EI} \tag{13}$$

where the initial curvature is given by

$$Z_o = -\sum_{n=1}^{\infty} H_n \sin(n\pi x/L) \tag{14}$$

If P has the opposite sign, the governing equation becomes that of buckling of a beam[19] with initial curvature, i. e.

$$\frac{d^2Z_1}{dx^2} + \frac{PZ_1}{EI} = -\frac{PZ_o}{EI} \tag{15}$$

The solution to eq. (13) with boundary conditions given by eq. (5) is

$$Z_1 = \sum_{n=1}^{\infty} \left[\frac{H_n \sin(n\pi x/L)}{1 + (n\pi/L)^2(EI/P)} \right] \tag{16}$$

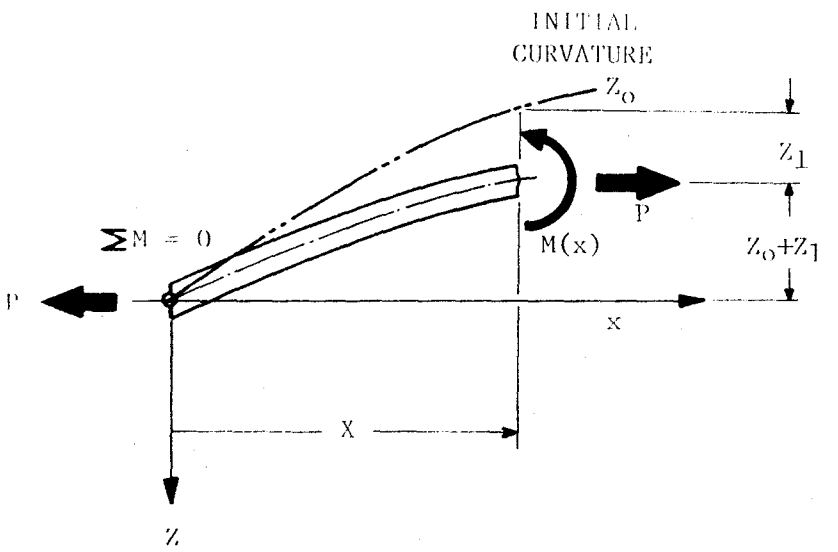

$$M(x) = EI \frac{d^2 Z_1}{d\,x^2}$$

$$\Sigma M = 0 = M(x) - P(Z_o+Z_1)$$

Fig. 4 Moment Equilibrium in a Corrugated Beam without Matrix Material

IN-PHASE WAVY LAYER

If the effect of the difference in the Poisson's ratio between the wavy layer and the matrix layer is neglected, then the thickness ratio, $(h_2 - h_1)/h_1$, Fig. 5, may be assumed to be constant throughout the deformation. Therefore, the In-Phase wavy layer can be assumed to be a corrugated beam on an elastic foundation which carries only shear forces. The torsional spring constant, K_T, is determined by considering an arbitrary angular deformation of the matrix material, θ. In Fig. 5, the shear deformation of the matrix material is illustrated. (It should be noted that the small angle assumption is made in the kinematics.)

$$K_T = \frac{\Delta T/\Delta x}{\theta} = 2(h_2-h_1)\, G_{XZ} = \text{constant} \tag{17}$$

From Fig. 5, $\alpha = h_2/(h_2-h_1) = 1/(1-v_f)$. Therefore eq. (7) reduces to

$$EI\frac{d^4Z_1}{d\,x^4} - \left\{P+K_T\left[\frac{h_2}{h_2-h_1}\right]^2\right\}\frac{d^2Z_1}{d\,x^2} = P\frac{d^2Z_o}{d\,x^2} \tag{18}$$

Using the initial geometry and boundary conditions given by eq. (14) and eq. (5), we obtain the vertical displacement of the In-Phase wavy layer given by

$$Z_1 = \sum_{n=1}^{\infty} \left[\frac{H_n \sin(n\pi x/L)}{1 + (K_T/P)[h_2/(h_2-h_1)]^2 + (n\pi/L)^2(EI/P)} \right] \tag{19}$$

From equations (8), (9) and (10), we easily obtain compact analytical solutions to the strains for an In-Phase wavy layer where the initial geometry is given by a one term sine function as follows:

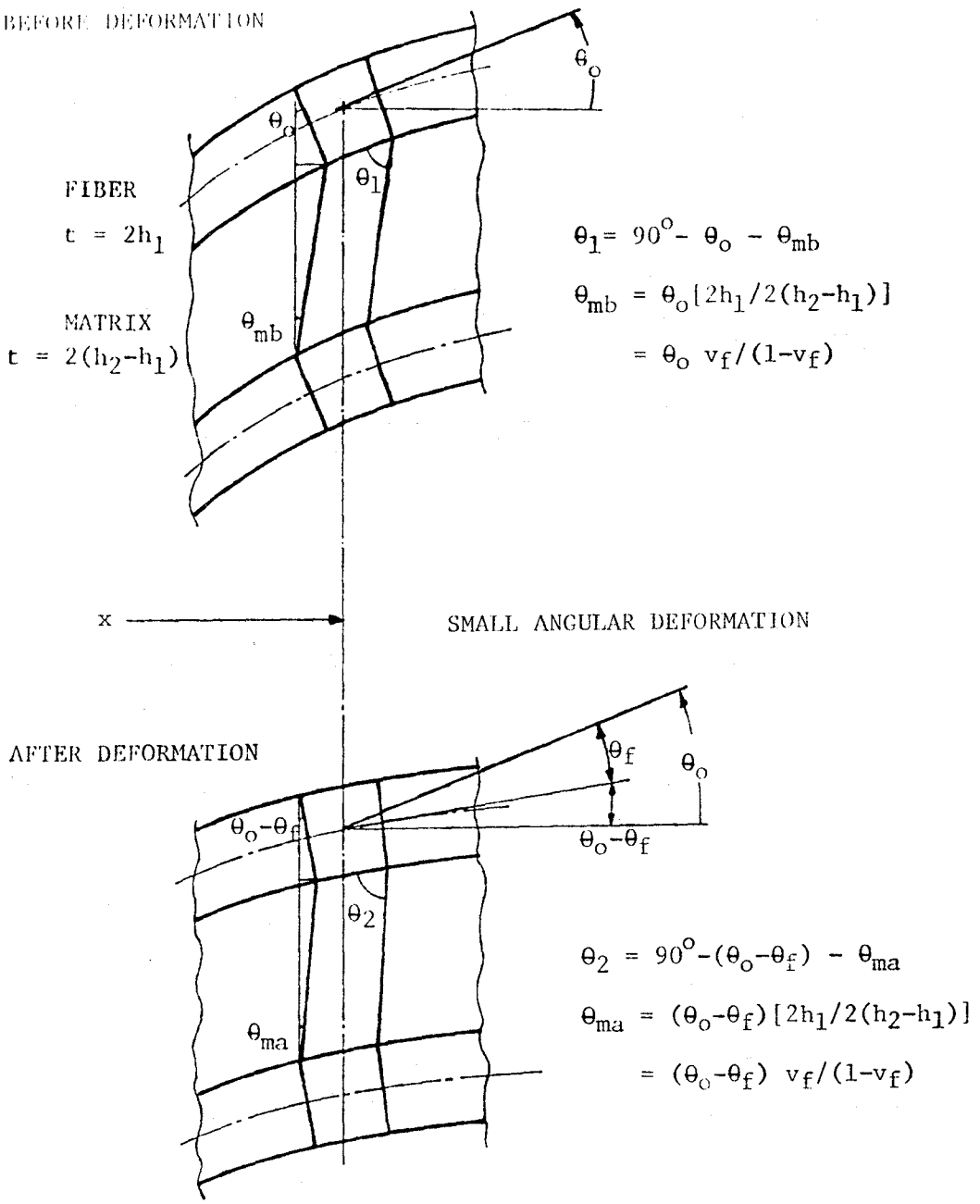

θ_m = SHEAR DEFORMATION OF THE MATRIX MATERIAL

$$\theta_m = \theta_2 - \theta_1 = \theta_f/(1-v_f) \quad , \quad \theta_f = dZ_1/dx$$

Fig. 5 Deformation of the Matrix Material Due to Stretching of the Initial Curvature of the Main Load-Carrying Layers(In-Phase)

Let

$$Z_o = -H_o \sin(\pi x/L) \tag{20}$$

then

$$\epsilon_{xx} = \epsilon_o - Z \frac{H_o (\pi/L)^2 \sin(\pi x/L)}{1 + \dfrac{2h_2{}^2 G_{XZ}}{(h_2-h_1)P} + \dfrac{(\pi/L)^2 EI}{P}} \tag{21}$$

$$\epsilon_{PS,AVE} = (\pi H_o/2L)^2 \frac{1 + \dfrac{4h_2{}^2 G_{XZ}}{(h_2-h_1)P} + \dfrac{2(\pi/L)^2 EI}{P}}{\left[1 + \dfrac{2h_2{}^2 G_{XZ}}{(h_2-h_1)P} + \dfrac{(\pi/L)^2 EI}{P} \right]^2} \tag{22-a}$$

$$\epsilon_{PS}(x) = \epsilon_{PS,AVE} [\ 1 + \cos(2\pi x/L)\ ] \tag{22-b}$$

These solutions are also valid for a single corrugated beam by setting $G_{XZ} = 0$.

For predicting the strain indicated by a standard extensometer measurement over one representing pitch,

$$\epsilon_{IND,AVE} = \epsilon_o + \epsilon_{PS,AVE} \tag{23}$$

For predicting the strains indicated by a full displacement field such as that obtained by moire interferometry,

$$\epsilon_{IND}(x) = \epsilon_{xx} + \epsilon_{PS}(x) \tag{24}$$

along the upper and lower surfaces of each wavy layer, where

$$-h_1 \leq Z \leq h_1$$

$$P = 2h_1 \; E \; \epsilon_o \; / \text{ unit width} \tag{25}$$

$$I = (2h_1)^3/12 = \frac{2}{3} h_1^3 \; / \text{ unit width.}$$

OUT-OF-PHASE WAVY LAYER

Since the straight lines AB and CD of the Out-of-Phase segment, Fig. 3b, remain straight after deformation, the Out-of Phase wavy layer can be assumed to be a corrugated beam on an elastic foundation which carries only tension-compression forces in the Z direction. The linear spring constant of the elastic foundation, as illustrated in Fig. 6, is given as a function of x. The upper and lower matrix layers of the representing segment are assumed to be two arrays of linear springs of different spring constants. Along the upper surface the length of the linear springs is given by

$$l_u = (h_2 - h_1) + H_o \sin(\pi x/L) \tag{26}$$

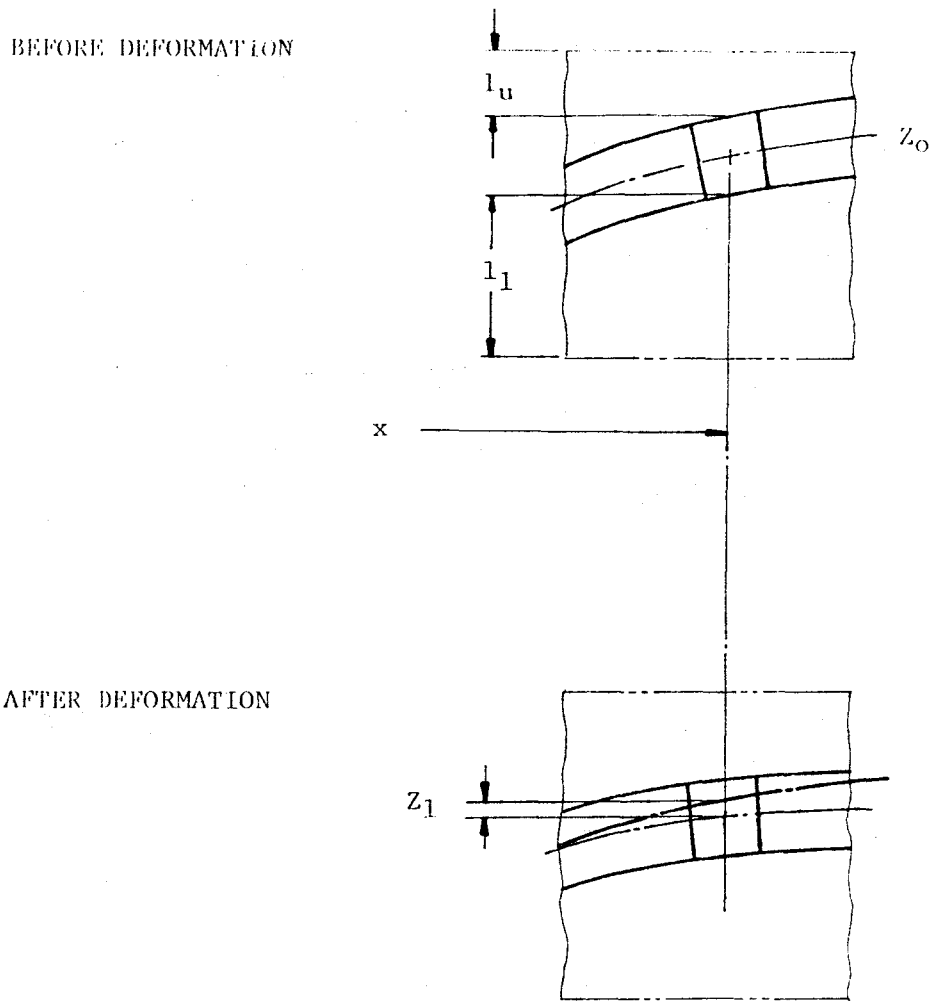

Fig. 6 Deformation of the Matrix Material Due to Stretching of the Initial Curvature of the Main Load-Carrying Layers (Out-of-Phase)

Along the lower surface,

$$l_1 = (h_2 - h_1) - H_o \sin(\pi x/L) \tag{27}$$

The equivalent spring constants of the upper and lower matrix material are given by

$$K_u = E_T/l_u \text{ and} \tag{28}$$

$$K_1 = E_T/l_1, \tag{29}$$

respectively.

Therefore, the total contribution of the matrix layer in one reseting segment can be replaced by a linear spring of which the spring constant is given by

$$K_L = K_u + K_1 ,$$

or

$$K_L(x) = \frac{2(h_2-h_1)\ E_T}{(h_2-h_1)^2 - H_o^2 \sin^2(\pi x/L)} \tag{30}$$

where the initial geometry is given by

$$Z_o = -H_o \sin(\pi x/L) . \tag{31}$$

Then the governing differential equation, eq. (7), becomes

$$EI\frac{d^4Z_1}{dx^4} - P\frac{d^2Z_1}{dx^2} + K_L(x)\,Z_1 = P\frac{d^2Z_o}{dx^2} \tag{32}$$

Since Z_1 should be symmetric with respect to $x = L/2$, we may assume

$$Z_1 = \sum_{\text{odd}} C_i \sin(i\pi x/L), \quad i = 1,3,5,\ldots,2n-1. \tag{33}$$

The principle of minimum potential energy may be expressed as

$$\partial\,\Pi/\partial\,C_i = 0 \quad \text{for all} \quad i = 1,3,5,\ldots,2n-1. \tag{34}$$

Substituting eq. (33) into eq. (1) and then applying eq. (34) yields n equations which are solved simultaneously for the unknown constants C_i. Table 1 shows that the four-term approximate solution is sufficient for the test cases considered herein.

RESULTS OF THE PARAMETER STUDY

Using eqs. (16), (19), (23), and (8-10), the indicated and actual strains for the three cases described above can be expressed in terms of the far-field strain, ϵ_o, which is the equivalent strain in a straight layer under the same loading conditions; thus the ratio between the reference strain and the far-field strain is always one. The maximum value of actual strain and the indicated(extensometer) strain are predicted and illustrated in Figs. 7-9. Three different combinations of geometric parameters of a single corrugated beam, an In-Phase layer, an Out-of-Phase layer are used as input data for three different material configurations. Also, the predicted variations of

Table 1 Comparison of Constants(C_i) for Out-of-Phase Configurations

r	E_T	G_{XZ}	L	h_1	h_2	H_o	C_1	C_3	C_5	C_7
20	1	0.5	20	2	8	4	-1.23E-02	-1.60E-04	3.01E-06	-1.14E-07
10	1	0.5	20	2	8	4	-6.53E-03	-1.58E-04	2.93E-06	-1.11E-07
3	1	0.5	20	2	8	4	-2.06E-03	-1.24E-04	2.19E-06	-8.17E-08
10.5	0.44	0.163	0.51	0.015	0.050	0.015	-5.47E-06	-2.64E-07	7.72E-10	-7.66E-12
10.5	0.44	0.163	0.51	0.015	0.275	0.078	-2.28E-04	-3.05E-06	8.19E-09	-4.87E-11
10.5	0.44	0.163	0.51	0.024	0.100	0.030	-3.84E-05	-8.98E-07	4.25E-09	-4.45E-11

$$Z_1 = C_1\sin(\pi x/L) + C_3\sin(3\pi x/L) + C_5\sin(5\pi x/L) + C_7\sin(7\pi x/L)$$

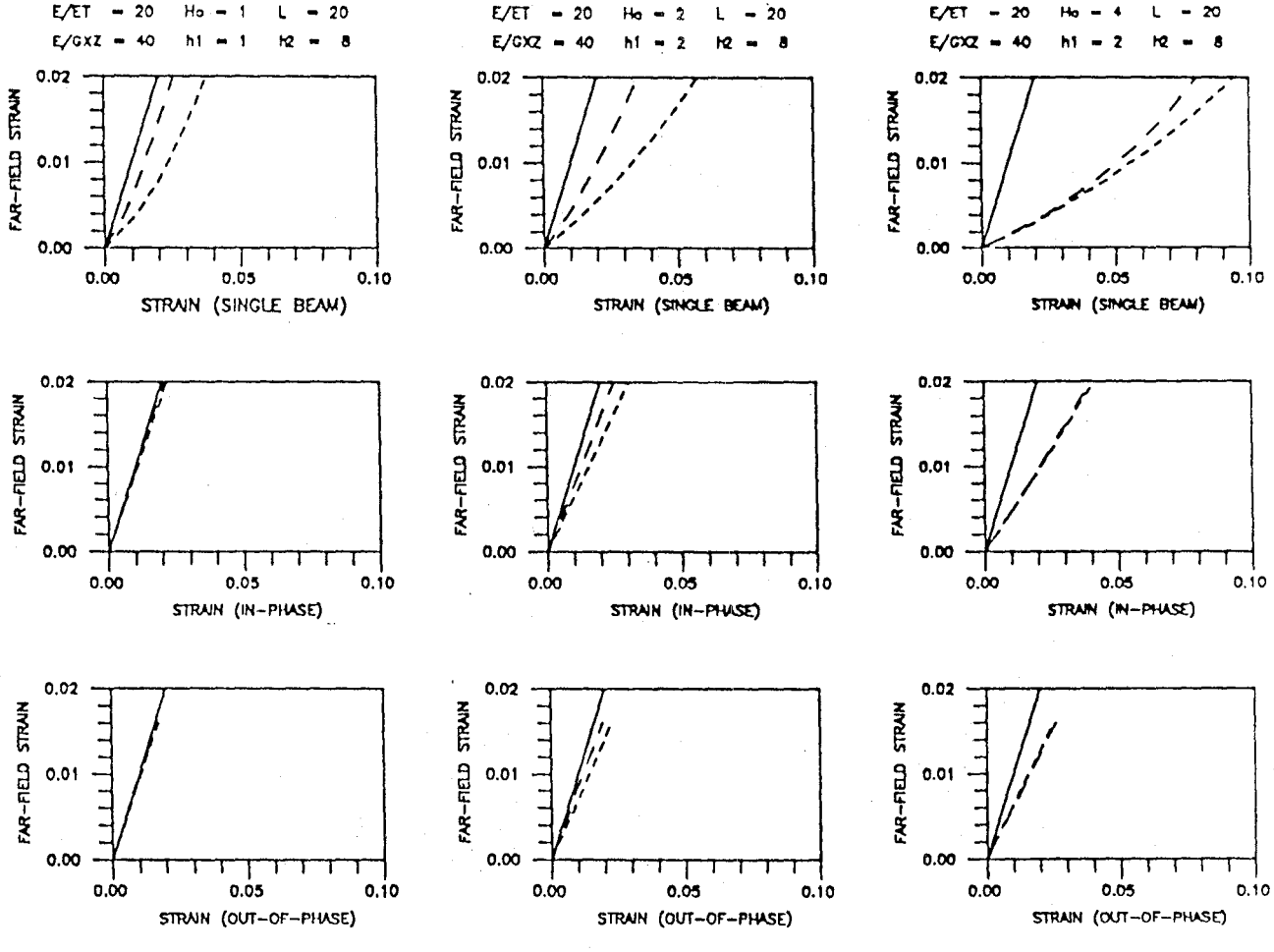

Fig. 7 Predicted Strain

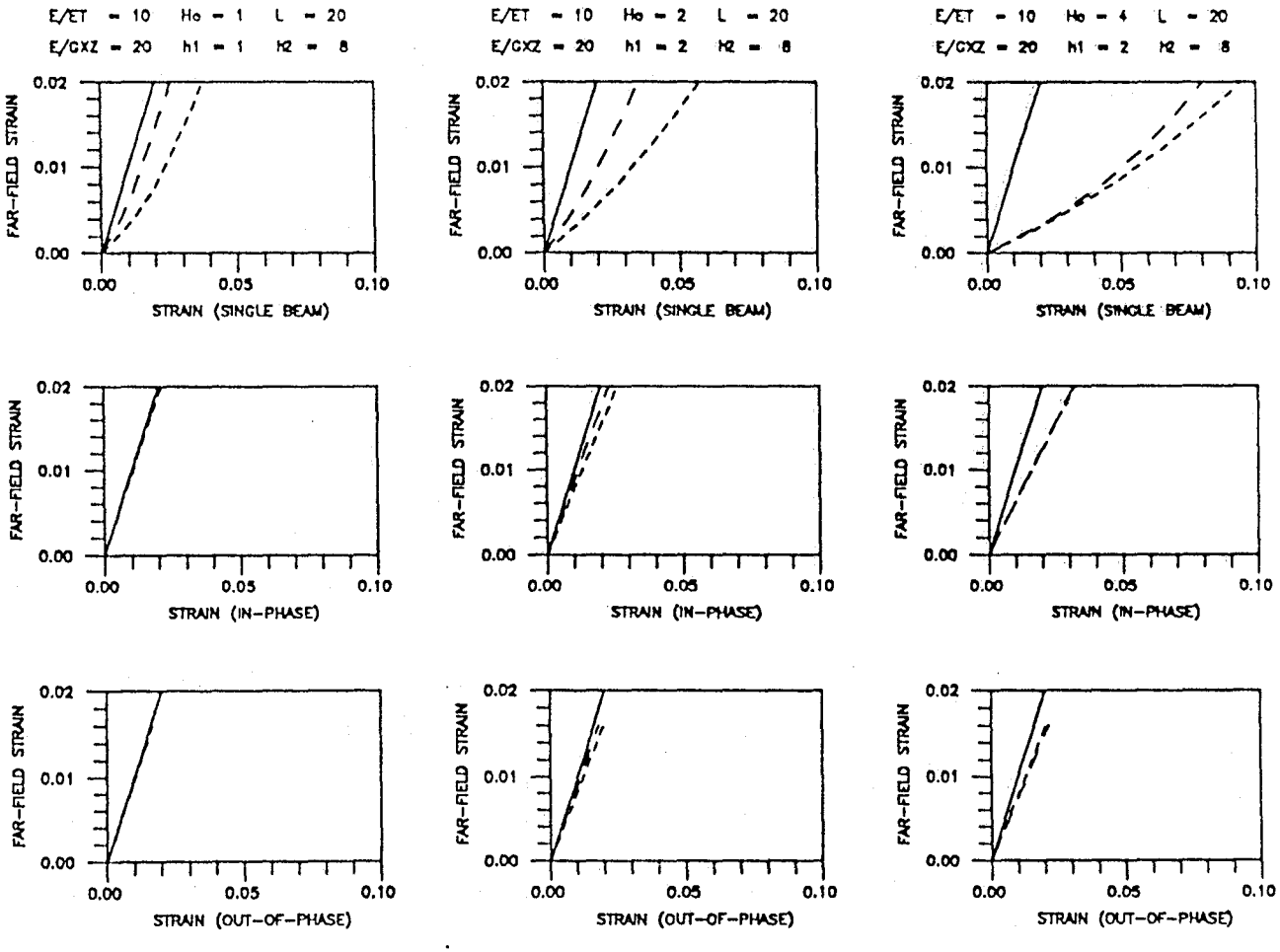

Fig. 8 Predicted Strain

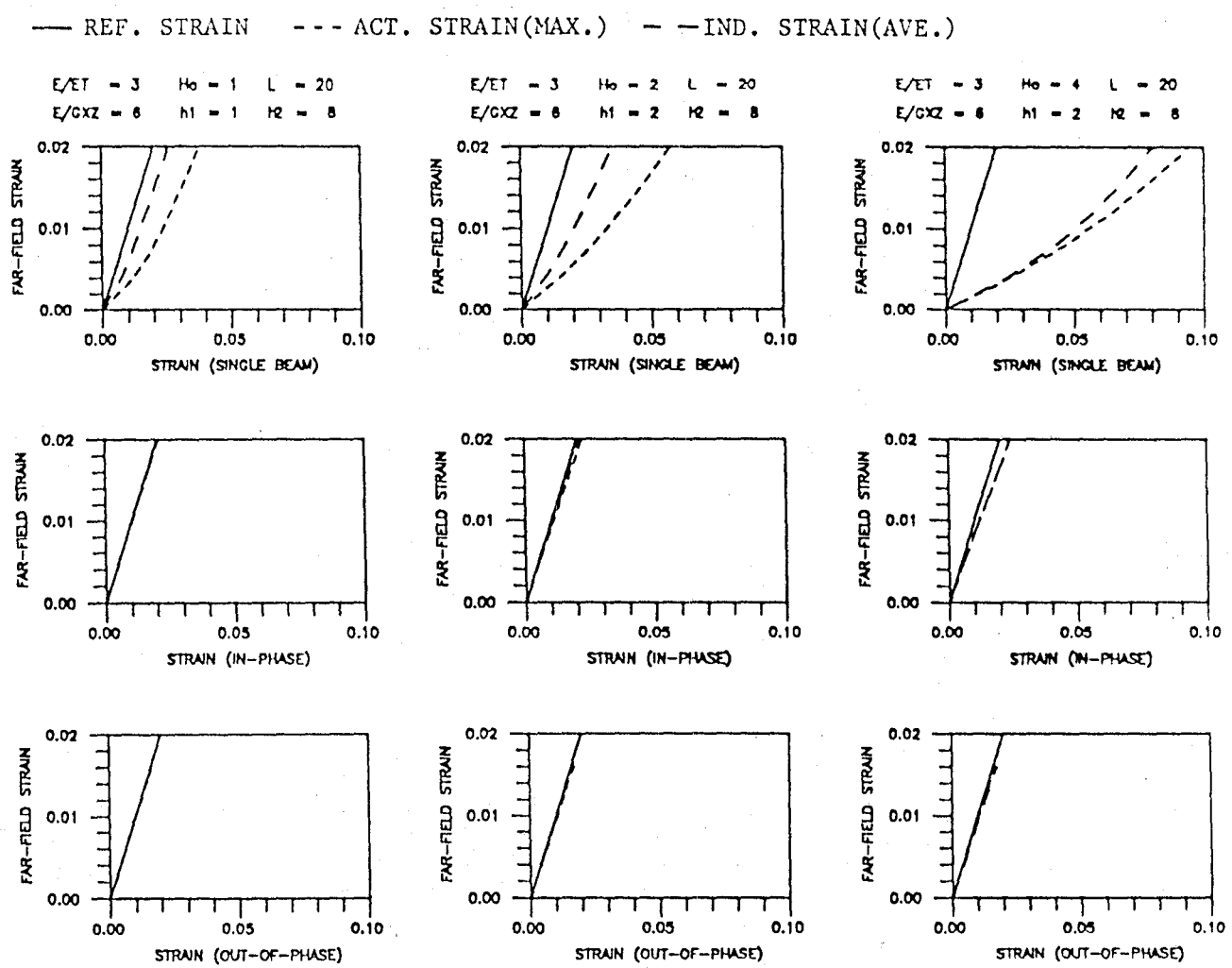

Fig. 9 Predicted Strain

the actual strain and observable strain which may be obtained experimentally from moire fringe analysis are plotted along the upper surface of the wavy layer in Figs. 10-12. The combinations of the geometric and material parameters in Figs. 10-12 are the same as in Figs. 7-9.

This parametric study shows the influence of wavy patterns and material properties on the indicated strain, or equivalently the effective Young's modulus. As an example, let's consider two laminated specimens with different main load-carrying materials. If both specimens have the same wavy pattern, the specimen with stiffer main load-carrying layers will exhibit more stiffness loss in the loading direction. It is also obvious that the In-Phase wavy layers exhibit larger deviations from the response of straight layers than do the Out-of-Phase wavy layers.

In Figs. 7-9, the reference strain, ϵ_o, the maximum value of the actual strain, $(\epsilon_{xx})_{MAX}$, and the average value of the indicated strain, $\epsilon_{IND,AVE}$, are plotted. Of these values, $\epsilon_{IND,AVE}$ can be directly measured from a specimen where the strain is measured by an extensometer over one pitch length of the wavy pattern. However, the bending stain, $(\epsilon_{xx}-\epsilon_o)$, must be confirmed by a full displacement field technique, such as moire interferometry. Also, the main assumptions of the model, i.e. the derivation of the spring constants for the matrix material surrounding the In-Phase and Out-of-Phase wavy layers, can be checked by moire interferometry.

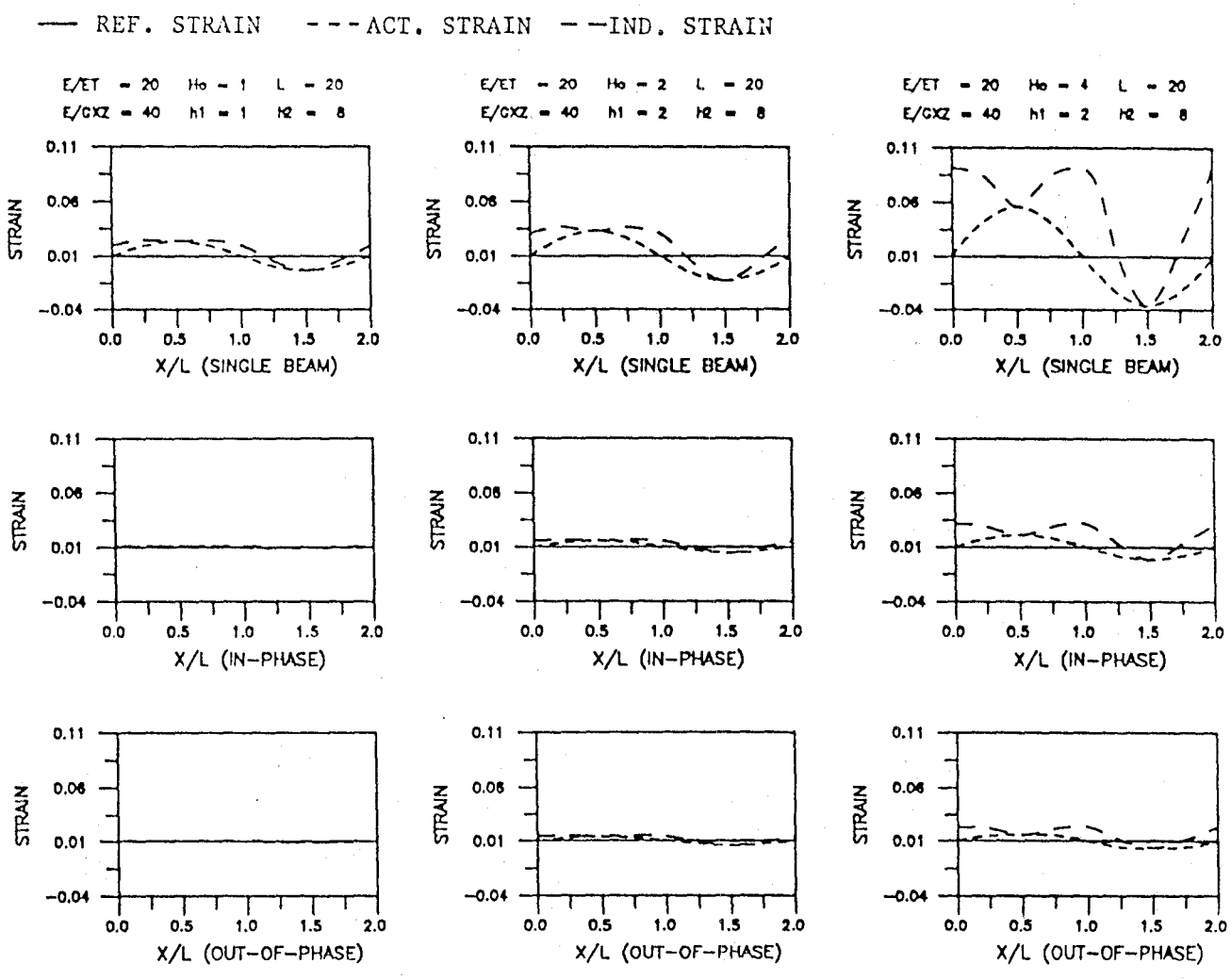

Fig. 10 Strain Variation along the Curvature

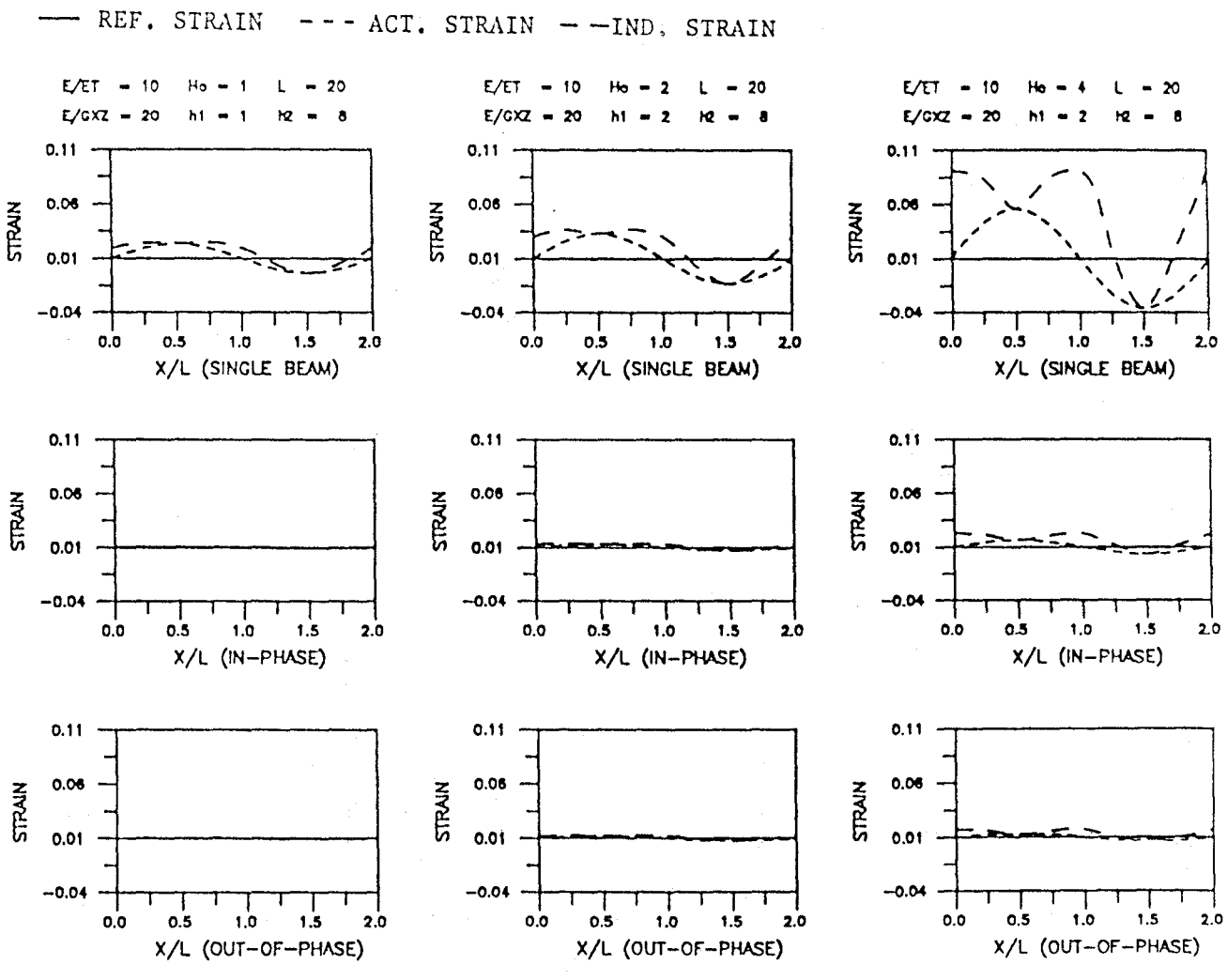

Fig. 11 Strain Variation along the Curvature

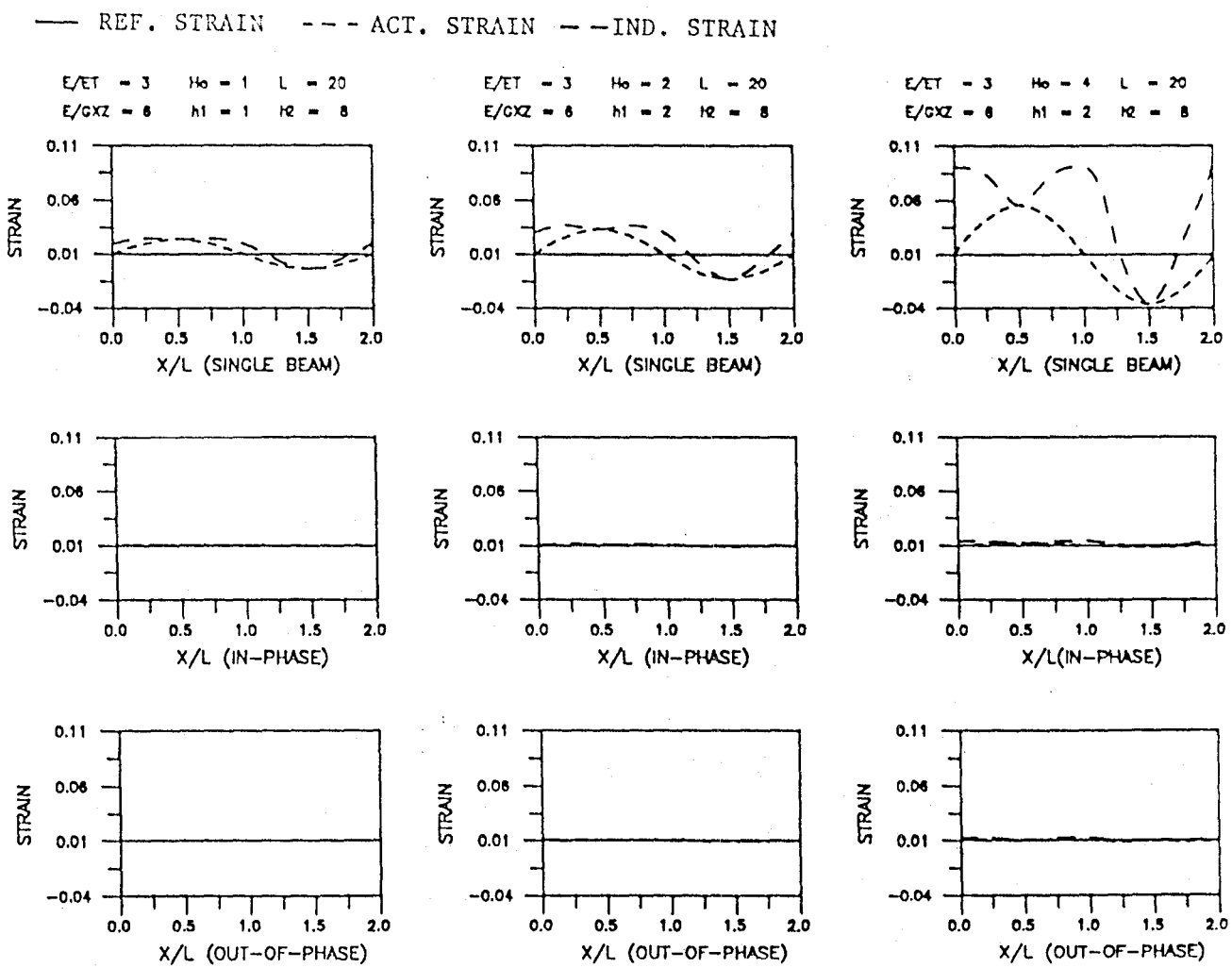

Fig. 12 Strain Variation along the Curvature

EXPERIMENTAL PROGRAM

An experimental program was conducted to verify the accuracy of the proposed mathematical model. Tensile specimens for each model type were prepared from aluminum 6061-T6 sheets of 0.76 mm (0.03 in.), 1.20 mm (0.047 in.), and 1.52 mm (0.06 in.) thicknesses, and room temperature curing epoxy. These materials were selected because of the necessity to fabricate precise wavy patterns in the main load-carrying layers. The dimensions of each specimen and the mechanical properties are given in Table. 2 and 3. The effective Young's moduli were measured by a one inch extensometer and the bending strains along the wavy aluminum layers were calculated from the analysis of the fringe pattern obtained from moire interferometry. Further details of the specimen preparation and experimental program are given in the following section.

MATERIAL PROPERTIES OF RAW MATERIALS

Using the average of three to five replicated tension tests conducted on an MTS testing machine and using a one inch extensometer, the Young's modulus of straight aluminum specimens was found to be 72.4 GPa (10.5 Msi). The Young's modulus and the Poisson's ratio of the epoxy were 3.034 GPa (0.44 Msi) and 0.35, respectively. (The elastic constants of the epoxy were measured by an extensometer and a strain gage rosette.) The shear modulus of the epoxy was estimated as 1.124 GPa (0.163 Msi) from the isotropic relationship given by

$$G = E/2(1+\upsilon) \tag{35}$$

Table 2 Specimen Configurations

	Single Al Layer	In-Phase Wavy Layer		Out-of-Phase Wavy Layer	
Material	6061-T6	6061-T6	Safe-T-Poxy	6061-T6	Safe-T-Poxy
Thickness mm (in.)	0.76 (0.030) 1.20 (0.047) 1.52 (0.060)	2*0.76 (0.030) 2*0.76 (0.030)	3.81 (0.150) 9.27 (0.365)	3*0.76 (0.030) 3*1.20 (0.047)	11.3 (0.445) 7.4 (0.291)
Width	25.4 (1.0)	25.4 (1.0)	25.4 (1.0)	25.4 (1.0)	25.4 (1.0)
Max. Rise, Ho mm (in.)	1.93 (0.076) 1.98 (0.078)	1.98 (0.078)		1.98 (0.078) 0.99 (0.039)	
Pitch = 2L mm (in.)	25.9 (1.02)				
Function of Wavy Pattern	Zo = Ho sin(x/L)				

Table 3 Measured Effective Young's Modulus

Fig. No.	Young's Modulus			
	Effective	Gpa (Msi)	Far-Field	Gpa (Msi)
Single Al Layers				
28-a	2.175	(0.374)	72.4	(10.50)
28-b	5.042	(0.731)	69.71	(10.11)
28-c	5.763	(0.836)	74.40	(10.79)
In-Phase Specimens				
29-a	8.695	(1.261)	21.95	(3.18)*
29-b	6.026	(0.874)	13.06	(1.894)*
Out-of-Phase Specimens				
30-a	9.998	(1.450)	14.70	(2.132)*
30-b	23.920	(3.469)	28.437	(4.124)*

* Obtained from the rule-of-mixture.

SPECIMEN PREPARATION FOR TENSION TEST

To prepare well-defined wavy patterns in aluminum layers, Fig. 13, the specially designed roller-press shown in Fig. 13 was used. Aluminum coupons of 25.4 mm (1 in.) width were pressed between the upper and lower rollers, equally spaced by one inch, so that the corrugated wavy patterns gradually became straight at both ends of the aluminum layer as shown in Fig. 14. The corrugated wavy patterns in aluminum layers were compared with mathematical sine curves and could be expressed in one-term sine functions of different coefficients of pitch and height. In Fig. 15, the comparison between a mathematical sine function and a corrugated aluminum layer is illustrated.

An epoxy ingot of Safe-T-Poxy was cured to prepare epoxy specimens. The volume ratio of the resin and hardener of the epoxy was seven to three. After the resin and hardener were thoroughly mixed, the temperature of the mixture was increased to 100^{o} F to remove air bubbles and cured at the same temperature for 24 hours. Epoxy coupons were cut from the cured epoxy ingot by a band-saw and then machined on a milling machine so that the final shapes are the straight coupon and the dogbone-type coupon. Then the specimen surfaces were polished to remove scratches and notches caused by cutting and machining. The epoxy ingot and two types of epoxy specimens are shown in Fig. 16.

The In-Phase and Out-of-Phase wavy laminate specimens were fabricated by bonding together the corrugated aluminum layers and the epoxy layers. Two different thicknesses of epoxy layer were prepared to measure the influence of the thickness of epoxy layers on the displacement fields of the In-Phase wavy specimens. Two different thicknesses of epoxy layer and aluminum layer were prepared for the Out-of-Phase

(a)

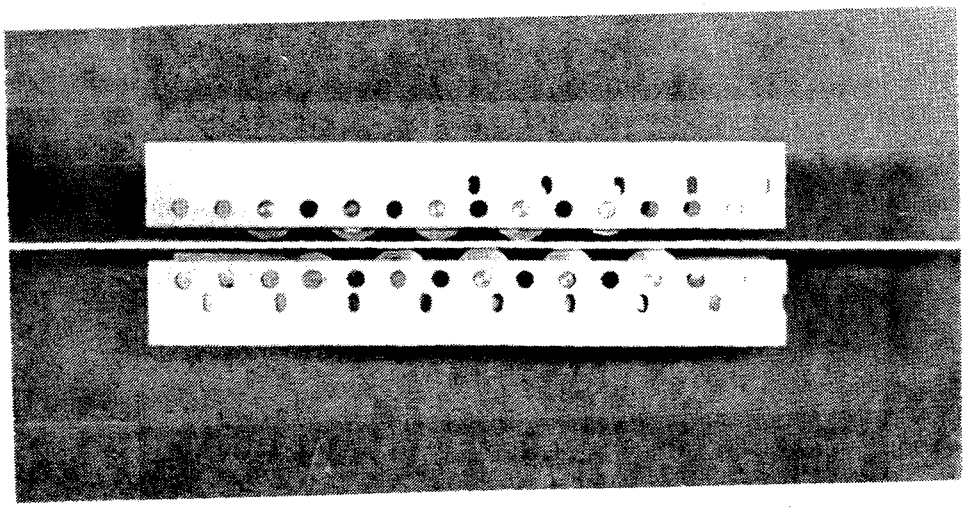

(b)

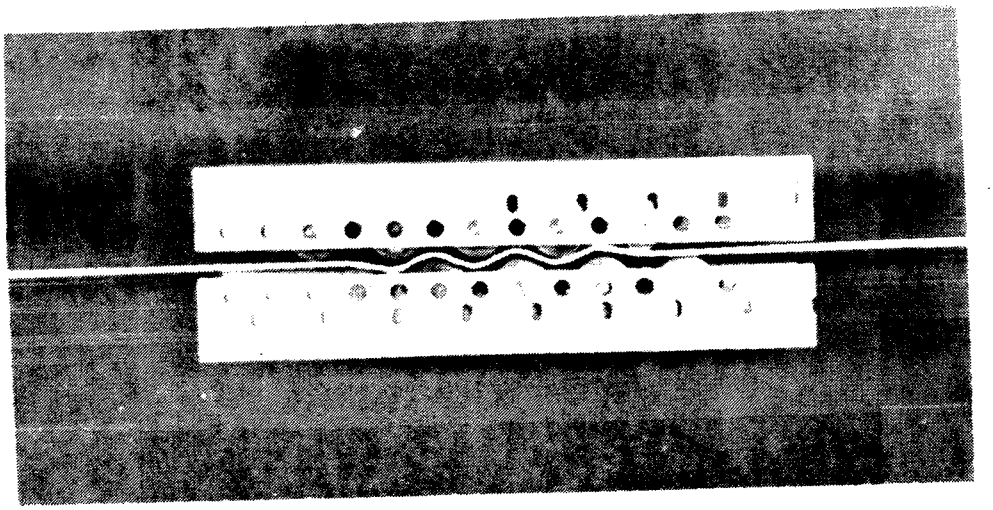

Fig. 13 Roller Press and Corrugating Procedure of Aluminum Layers

(a) Before Pressing
(b) After Pressing

(a)

(b)

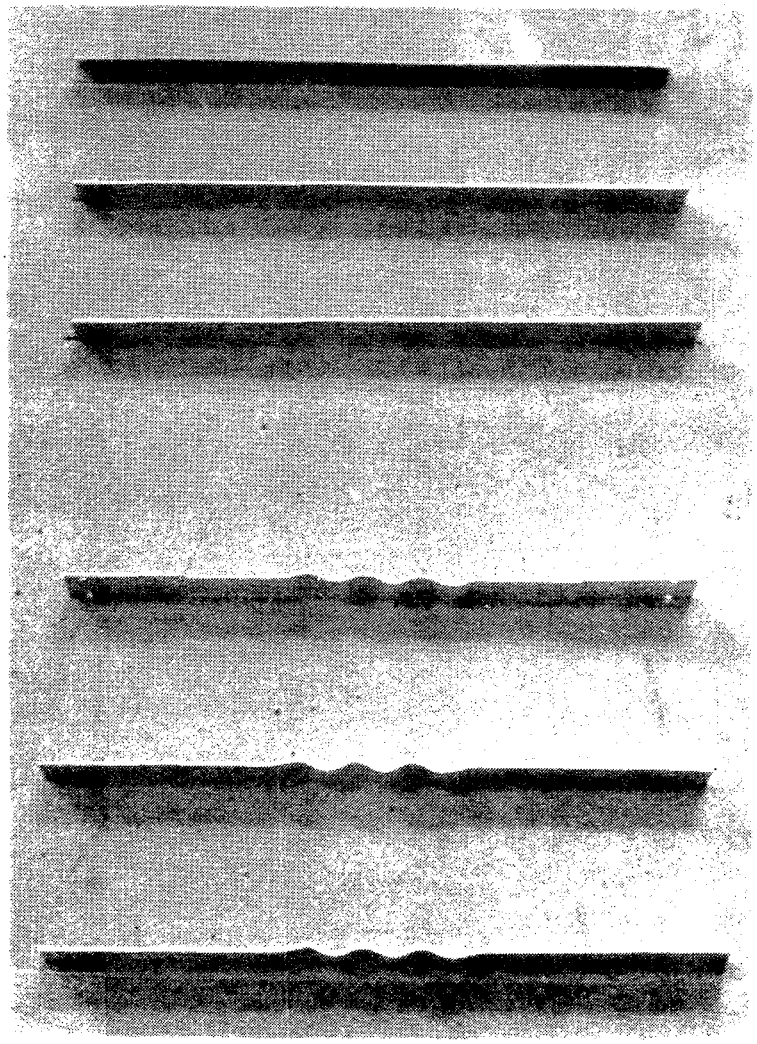

Fig. 14 Aluminum Layers of Different Thicknesses

(a) Straight Layers
(b) Corrugated Layers

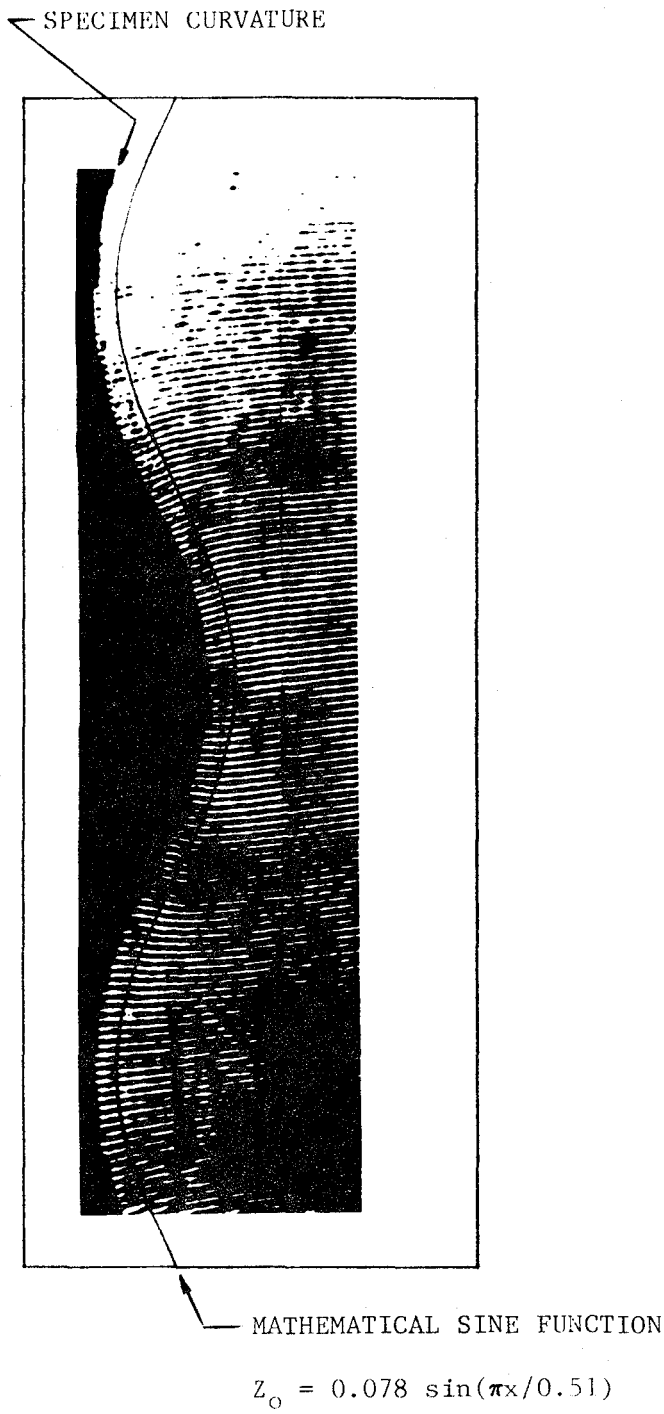

Fig. 15 Comparison between a Specimen Curvature and a Mathematical Sine Function

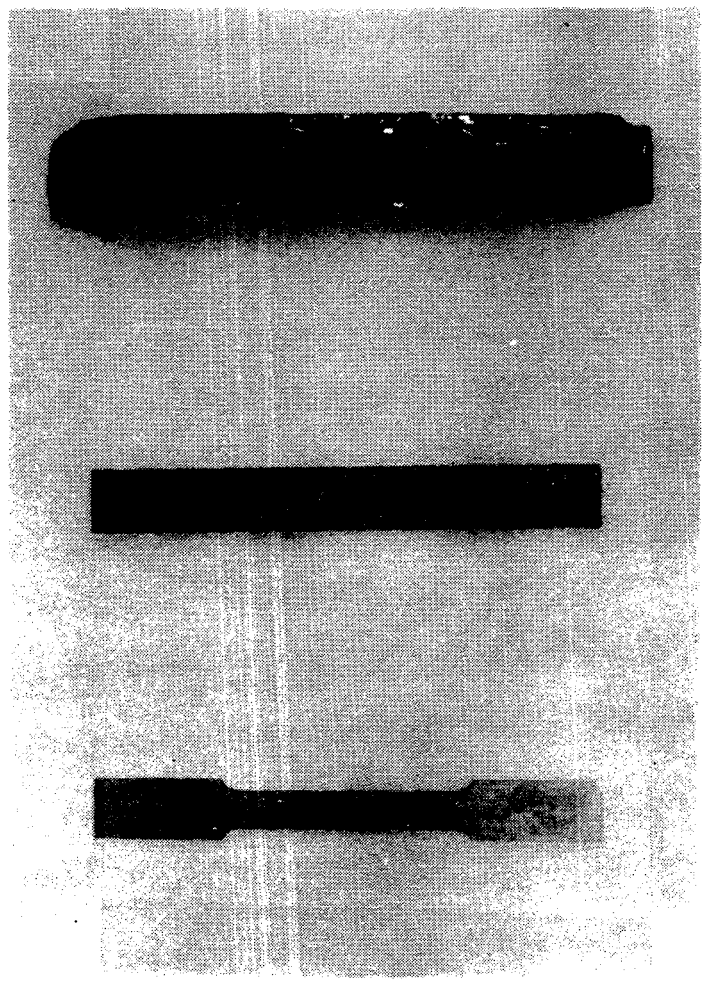

Fig. 16 Epoxy Ingot and Specimens

(a) Epoxy Ingot
(b) Straight Coupon
(c) Dogbone Coupon

wavy specimens. The corrugated aluminum layers for both laminates were surface-treated before bonding to improve the bond strength and to prevent any delamination during machining and tensile tests. Both surfaces of each aluminum layer were coated with acrylic resin. Spacers were inserted between coated aluminum layers to obtain gaps between each layer so that the Safe-T-Poxy filled up the gap between aluminum layers. After curing in an oven for 24 hours at 100° F, both free edges of each laminate were machined and polished to approximately one inch width. Some of the fabricated specimens with In-Phase and Out-of-phase wavy patterns are shown in Fig. 17.

Each specimen contained two or three aluminum layers with In-Phase or Out-of-Phase wavy patterns. Strictly speaking, each specimen does not exactly represent the mathematical model which has been developed for an infinite number of wavy layers. However, no attempt has been made to account for the finite thickness of the specimens.

TENSION TEST

All tension tests were conducted at a constant loading rate of 4.5 Kg/s (10 lb/s) or 9 Kg/s (20 lb/s) on an MTS machine . Strains were measured by a one inch extensometer which corresponds to one pitch length of the wavy patterns. The knife edges of the extensometer were placed in the machined grooves of two aluminum tabs glued on the convex points of the wavy patterns. The specimens were held in 51 mm (2 in.) wide wedge-action friction grips so that the specimen length between grip ends was approximately 125 mm (5 in.). To insure repeatability of the results, each specimen was loaded three to five times within its elastic limit. The specimen configurations of corrugated aluminum layers and In-Phase and Out-of-Phase wavy laminates were previously

(a)

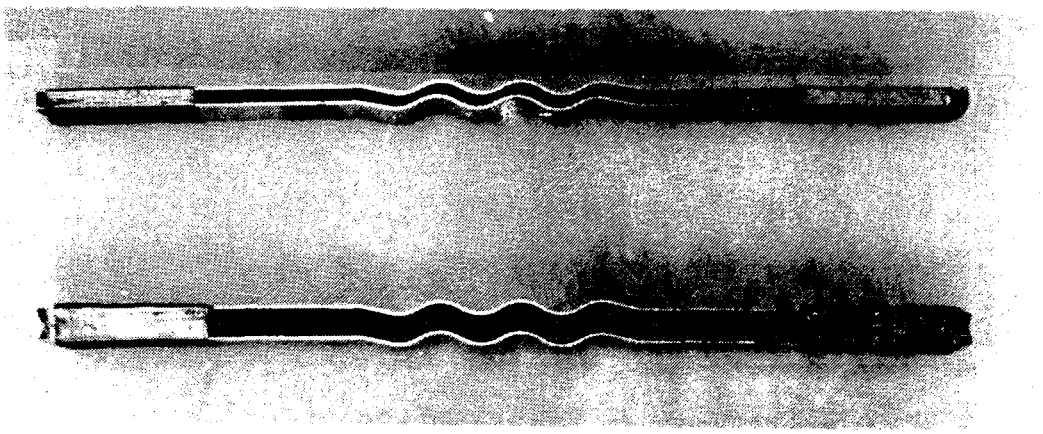

(b)

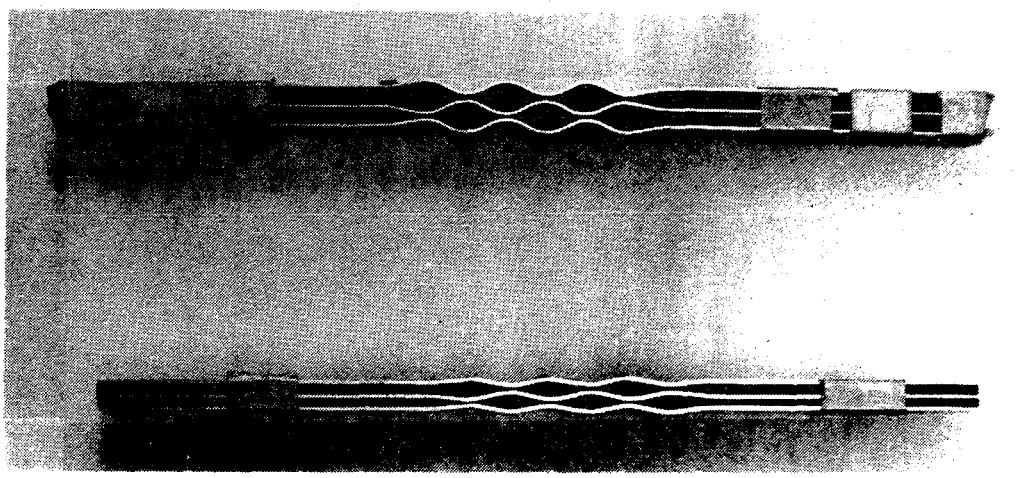

Fig. 17 Laminated Specimens

(a) In-Phase
(b) Out-of-Phase

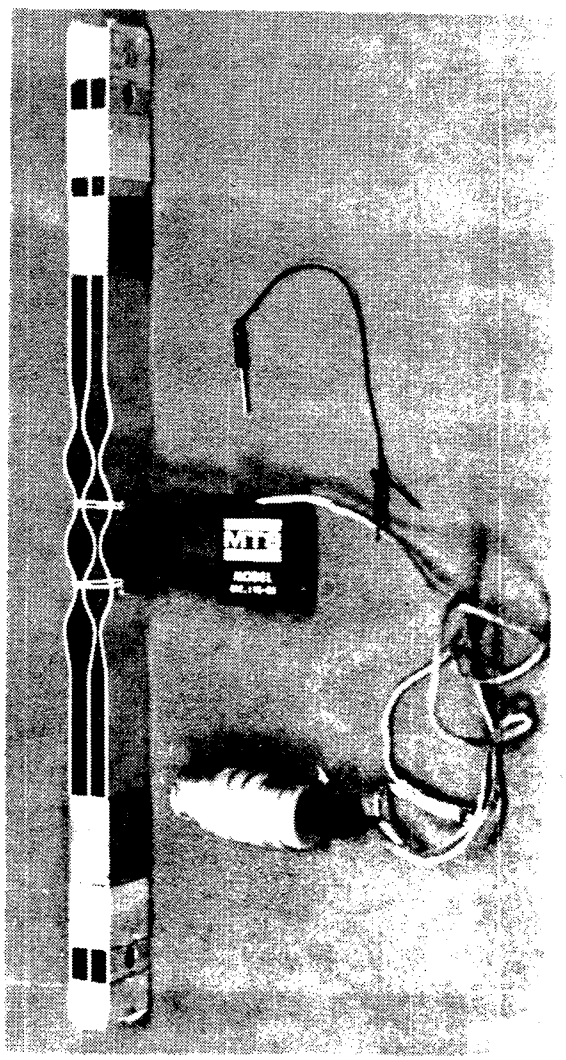

Fig. 18 Installment of the Extensometer on a Specimen

given in Table 2. Fig. 18 illustrates the extensometer installation for a typical specimen.

Values of the effective Young's modulus of each aluminum layer and wavy laminate configuration were obtained from the replicated tests by using the least square curve fitting technique to the digital test data. The Young's modulus of each specimen was nondimensionalized by dividing by the reference Young's modulus, i.e. the equivalent Young's modulus of the layer or laminate without corrugated wavy patterns. Measured values of the effective Young's modulus of each specimen configuration were previously given in Table 3.

SPECIMEN PREPARATION FOR MOIRE INTERFEROMETRY

Moire interferometry is a real time method that gives the in-plane displacements of the specimen surface below the moire grating. This technique does not require a transparent specimen as the conventional photoelasticity technique does. The Moire grating frequency for this study is 2400 lines/mm(60,960 lines/inch). Since the technique provides contour maps of in-plane displacement fields from a cross grating transferred to the specimen surface, it may be used for non-homogeneous materials. For more details of moire interferometry and the general procedure of specimen preparations, please refer to Post[15].

One In-Phase specimen and one Out-of-Phase specimen were prepared for moire interferometry. A moire grating supplied by Professor Daniel Post at VPI & SU was coated with a thin aluminum layer using a metal vaporizing technique and cut into appropriate sizes for the specimens. Mirrorized moire gratings were transferred to the specimen surfaces as shown in Fig. 19.

In order to use a hinge joint for applying tension loads to a spe-

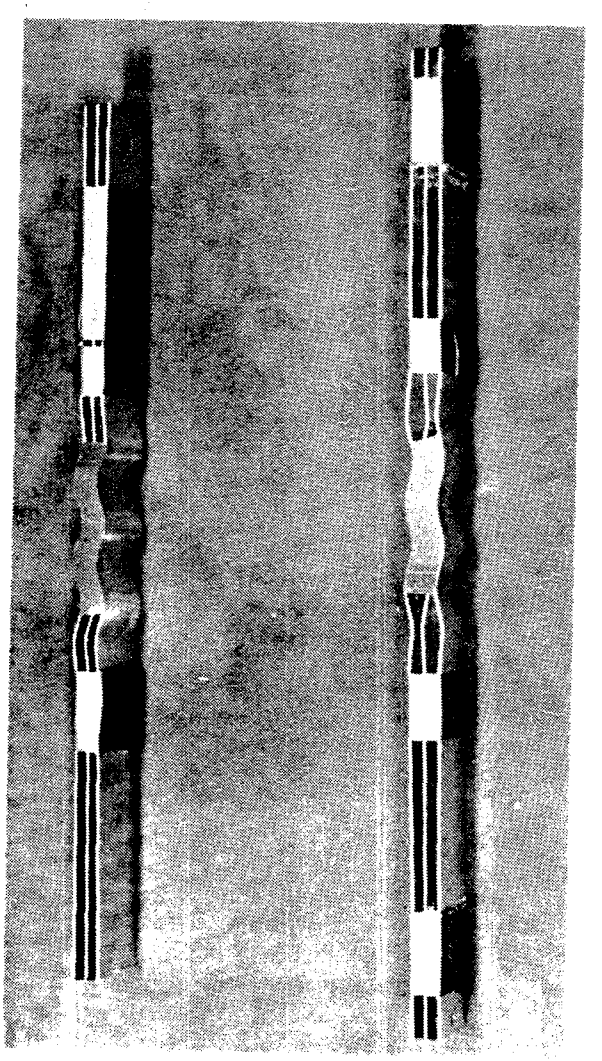

Fig. 19 Specimens with Moire Gratings

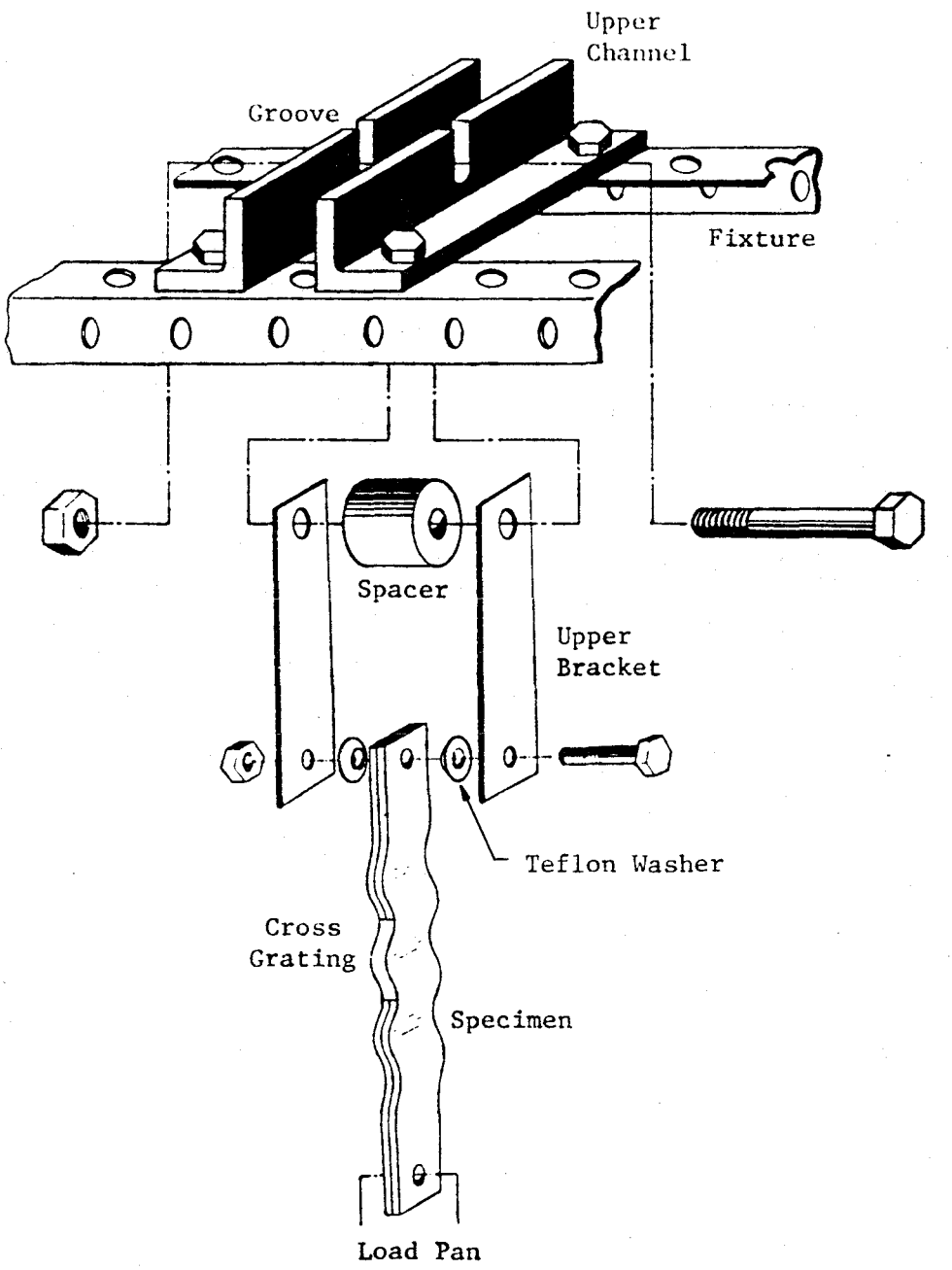

Fig. 20 Specimen Installation to the Fixture

cimen without causing global bending, a quarter inch diameter hole was drilled at each end of the specimen. Then, one end was connected to the load pan and the other end was connected to the upper brackets by quarter inch bolts as shown in Fig. 20. Teflon washers were placed between the outermost aluminum layers and the inner surfaces of the upper brackets to minimize friction forces between the brackets and the specimen. The upper brackets are connected to the grooves in the upper channels by a 5/16 inch bolt. Then, tension load is applied to the specimen by putting calibrated weights on the load pan. Fig. 21 shows the moire setup with a specimen installed in the test configuration.

MOIRE TEST

If the displacement in a specimen is large enough to neglect any possible misalignment during loading, then the strain components, ϵ_{xx} and ϵ_{ps} can be directly obtained from the loaded fringe patterns. However, the increment of the fringes due to tension loading was not so significant and the out-of-plane displacement was not negligible when compared to the in-plane displacement. Therefore, the mirrors in the test setup schematic of Fig. 22 were adjusted to increase the number of fringes at the zero loading condition to facilitate the measurement of the distance between each fringe and to obtain better contrast between the light and dark fringes in both the axial and transverse displacement fields. This initial carrier fringe pattern does not eliminate the coupling between the in-plane and out-of-plane displacements, but the bending strain component can be calculated from the axial fringe patterns with carrier fringes.

After the initial fringe patterns with the carrier fringes for the axial and transverse displacement fields were photographed from the

In-Phase specimen at zero loading condition, a 27 Kg (60 lb) tensile load was applied and both fringe patterns were photographed again. This procedure was repeated at 36 Kg (80 lb), 54 Kg (120 lb), and 72 Kg(160 lb) tensile loads. Then the horizontal and vertical mirrors were adjusted to reduce the fringes in both displacement fields so that the effect of the epoxy layers on the center aluminum layer could be qualitatively observed as illustrated in Fig. 23-c and 23-d. The load was removed and the same procedure was repeated with different initial carrier fringes in both axial and transverse displacement fields. These sets of photographs are shown in Figs. 23 and 24.

The Out-of-Phase specimen was photographed under zero, 36 Kg (80 lb), and 67.5 Kg (150 lb) for the axial displacement field, and under zero, 27 Kg (60 lb), 45 Kg (100 lb), and 67.6 Kg (150 lb) for the transverse displacement field. The sets of photographs taken from the Out-of-Phase specimen with different initial carrier patterns are shown in Figs. 25- 27.

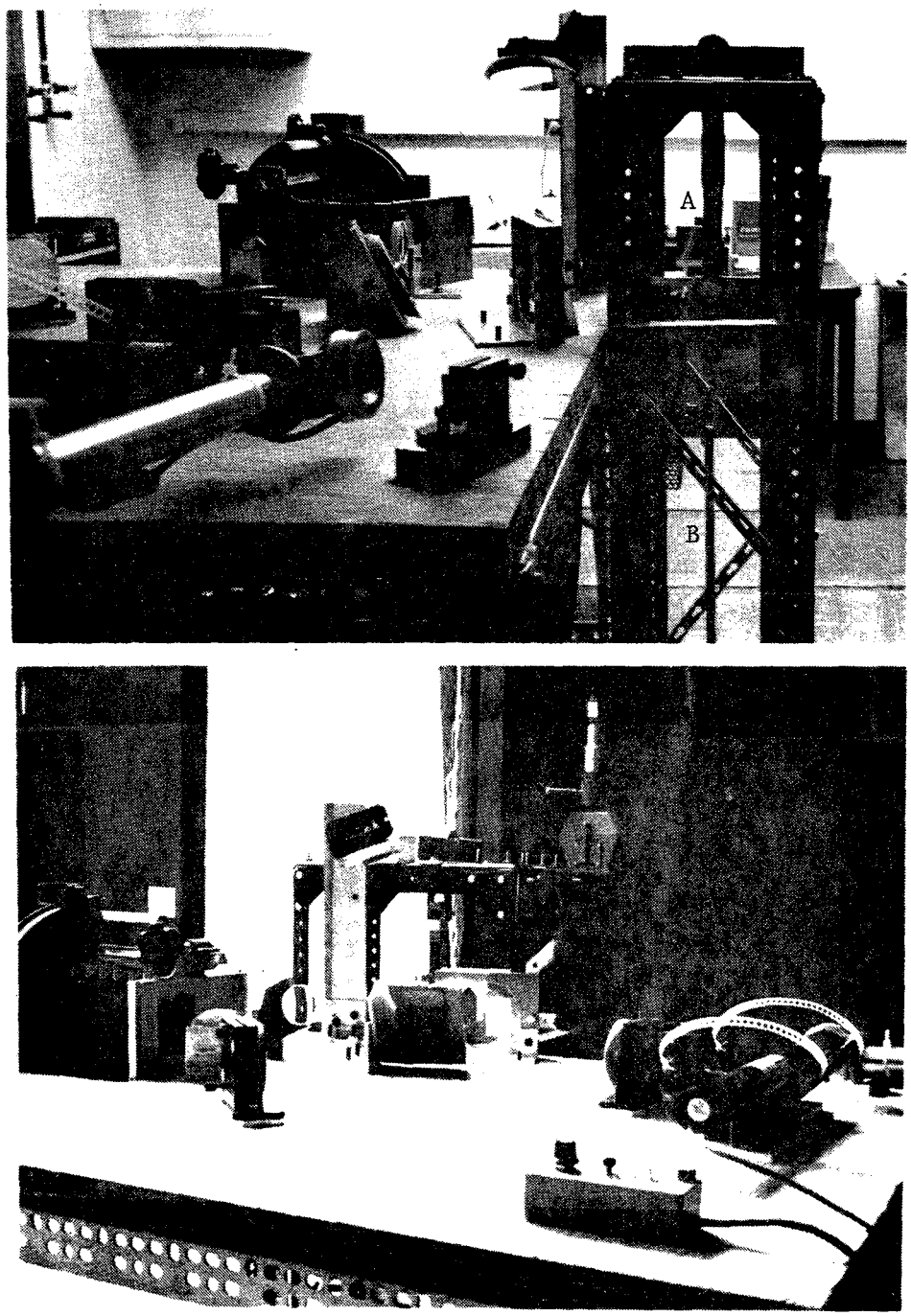

Fig. 21 Moire Equipment with Load Frame

A = Specimen
B = Load Panel

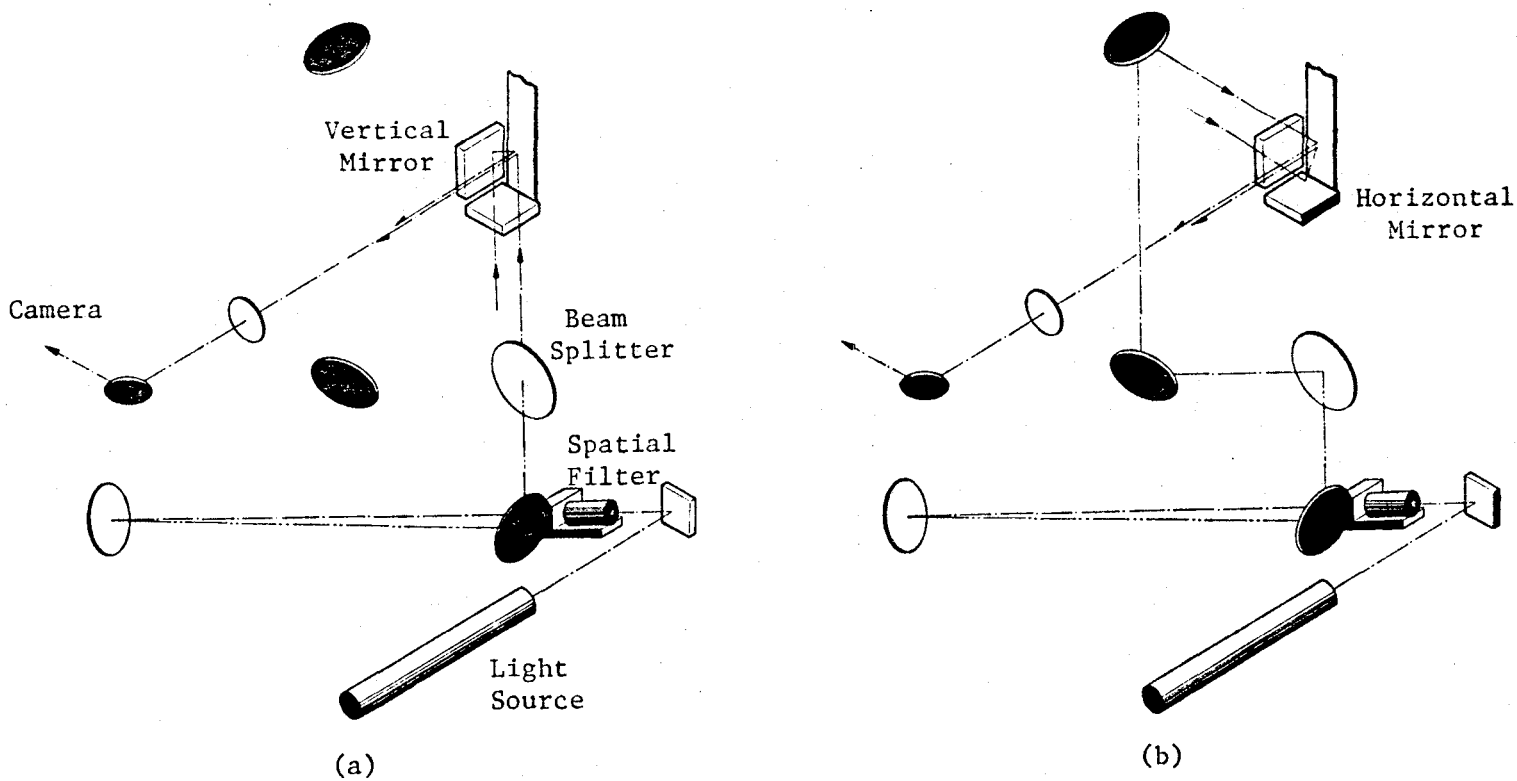

Fig. 22 Schematics of Moire Interferometry

(a) Transverse Field

(b) Axial Field

(a)

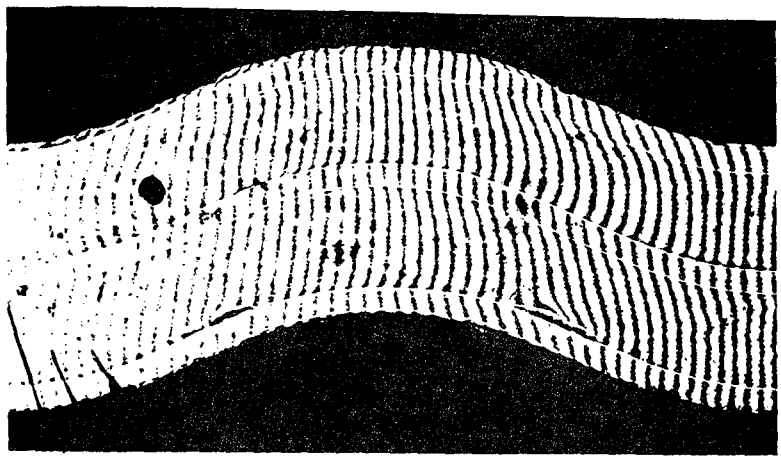

(b)

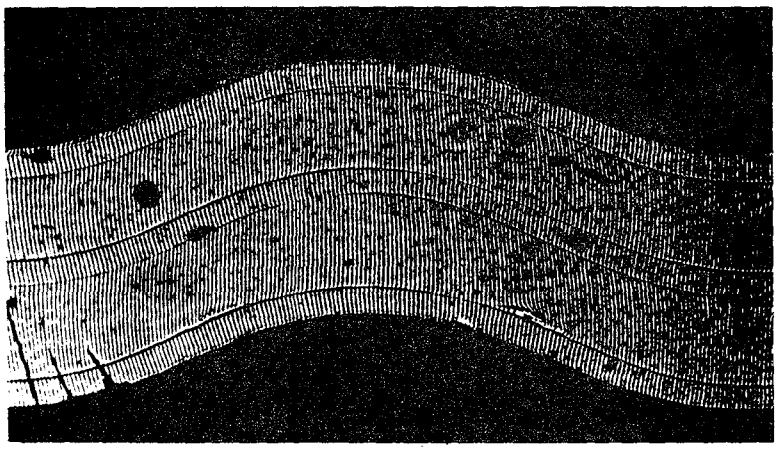

Fig. 23 Axial Fringe Patterns from an In-Phase Specimen

(a) 0 lb(with Carrier Fringes)
(b) 60 lb
(c) 120 lb
(d) 120 lb(with less Carrier Fringes)

Continued to Next Page

(c)

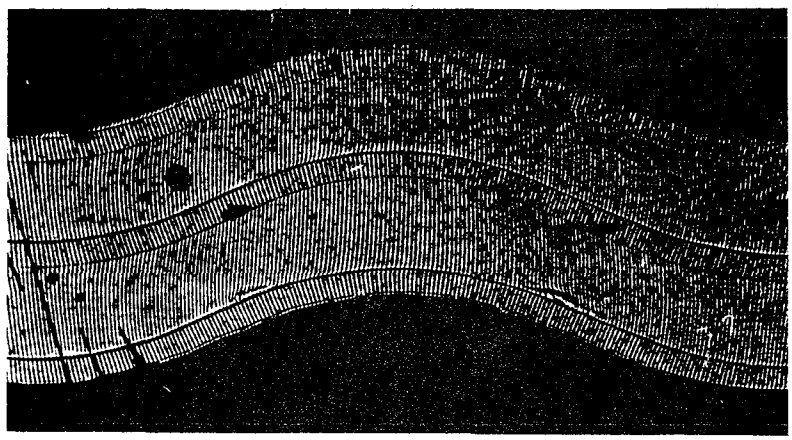

(d)

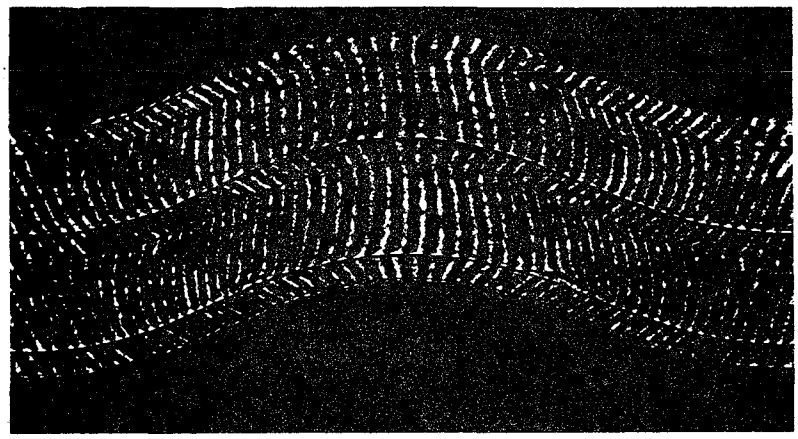

Fig. 23 (Continued)

(a)

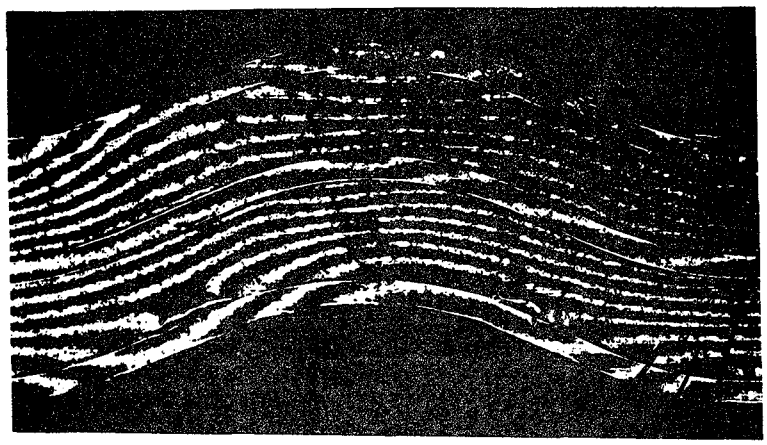

(b)

Fig. 24 Transverse Fringe Patterns from an In-Phase Specimen

(a) 0 lb(with Carrier Fringes)
(b) 60 lb(Increasing Load)
(c) 120 lb
(d) 120 lb(Nulled-Out)
(e) 60 lb(Decreasing Load)

Continued to Next Page

(c)

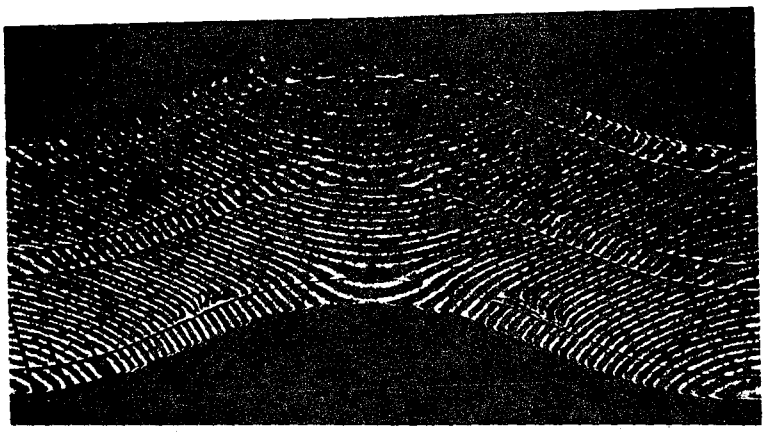

(d)

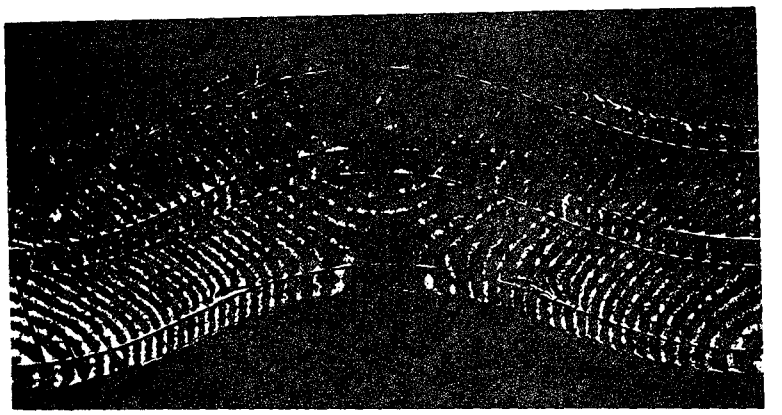

Fig. 24 (Continued)

Continued to Next Page

(e)

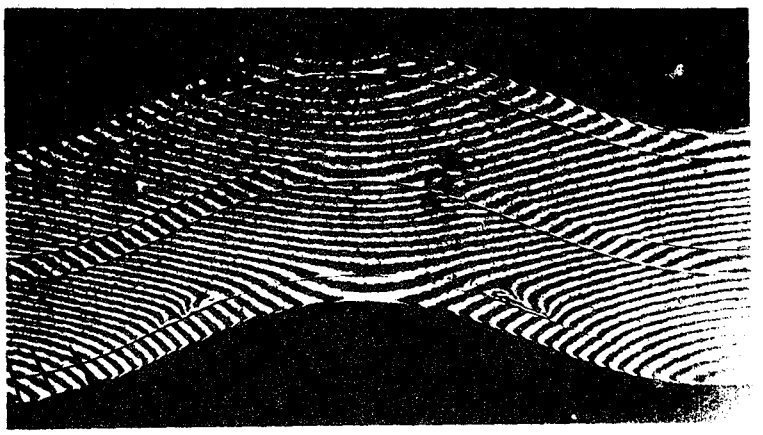

Fig. 24 (Continued)

(a)

(b)

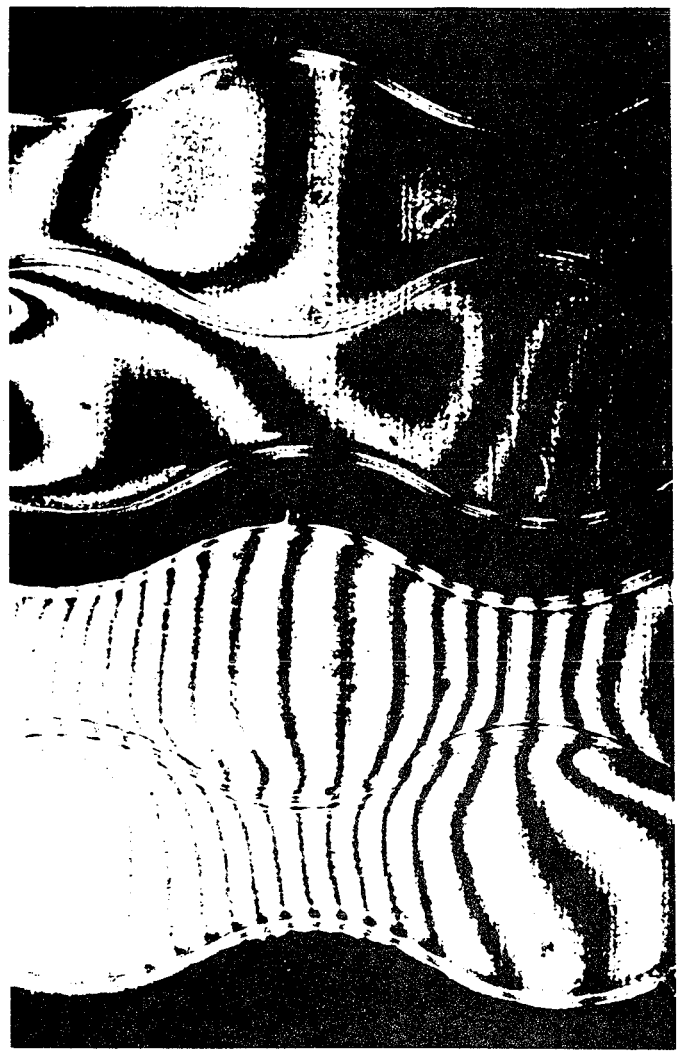

Fig. 25 Axial Fringe Patterns from an Out-of-Phase Specimen

(a) 0 lb(Nulled-Out)
(b) 0 lb(with Carrier Fringes)
(c) 80 lb
(d) 150 lb

Continued to Next Page

(c)

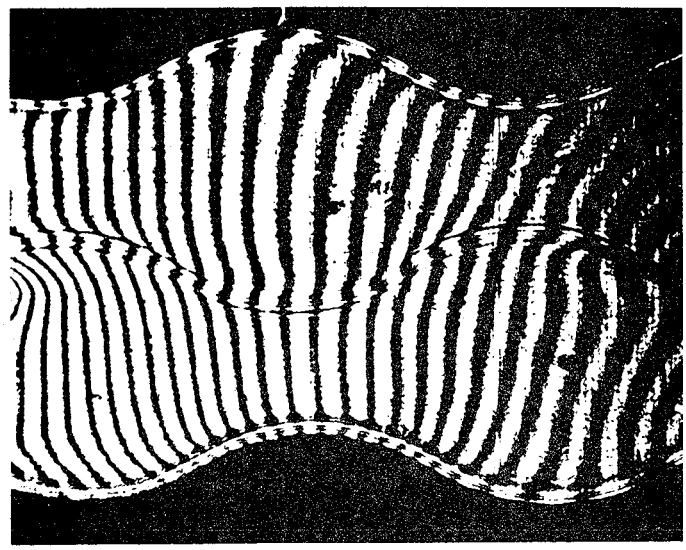

(d)

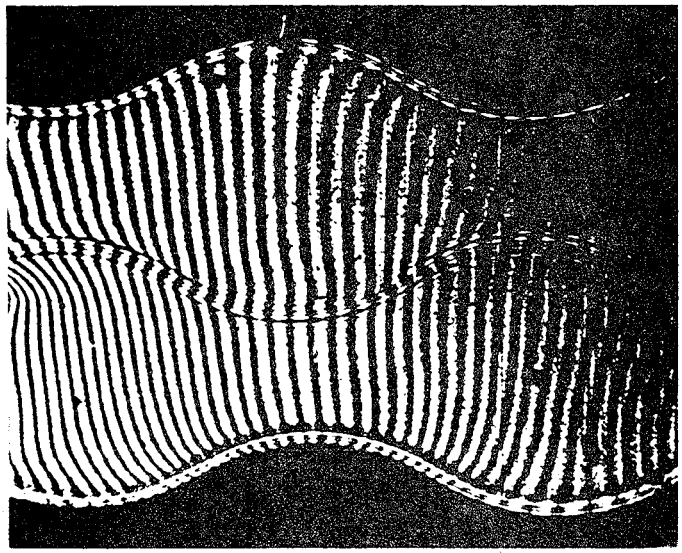

Fig. 25 (Continued)

(a)

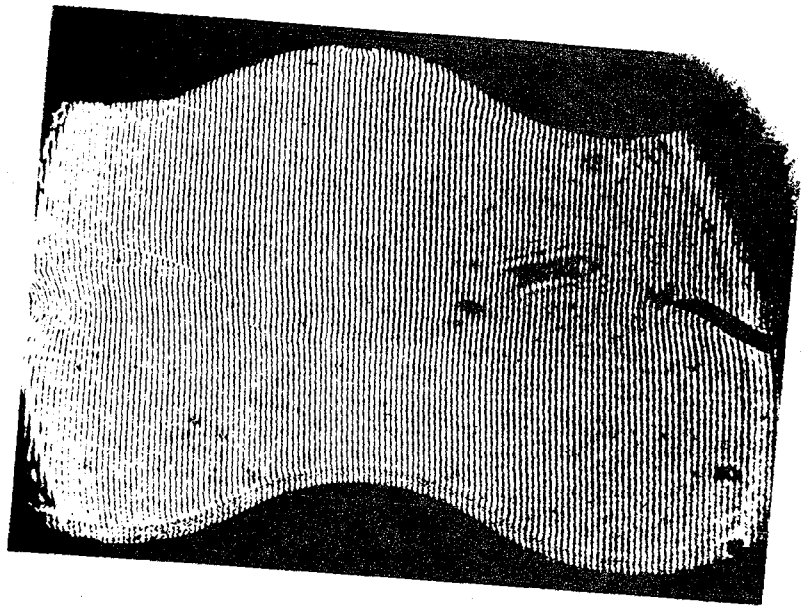

(b)

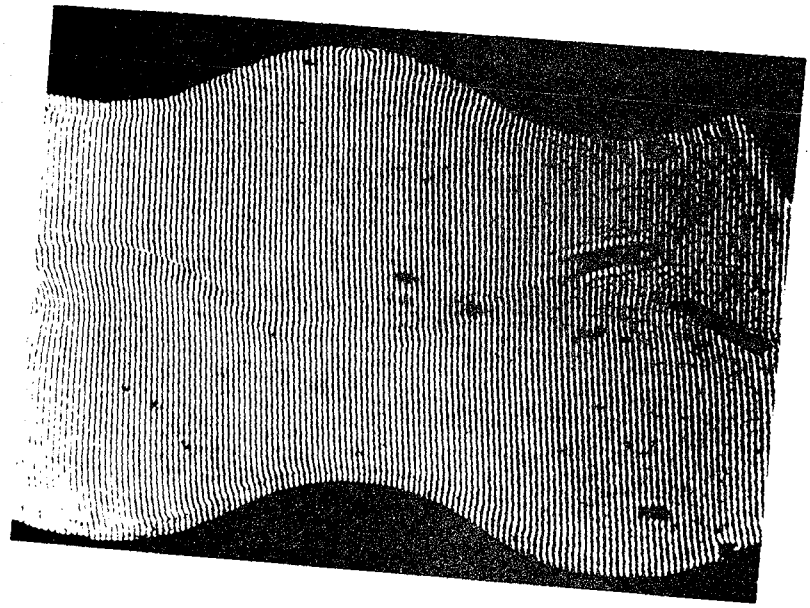

Fig. 26 Axial Fringe Patterns with More Carrier Fringes (Out-of-Phase)

(a) 0 lb
(b) 80 lb
(c) 150 lb

Continued to Next Page

(c)

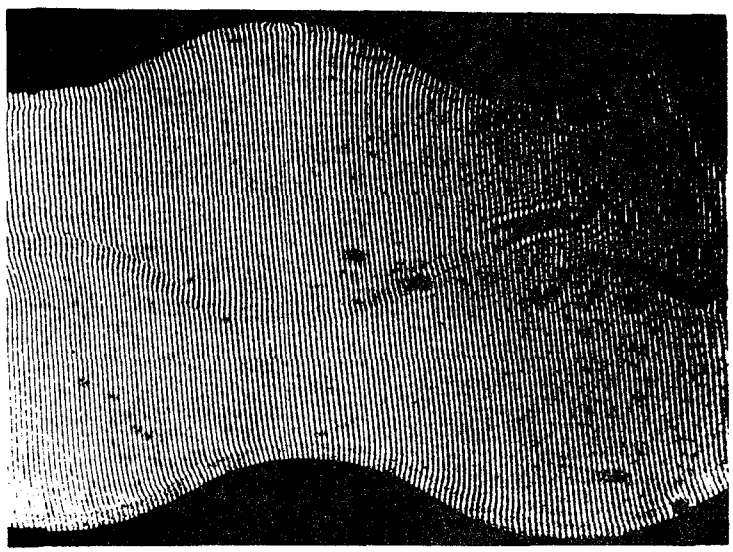

Fig. 26 (Continued)

(a)

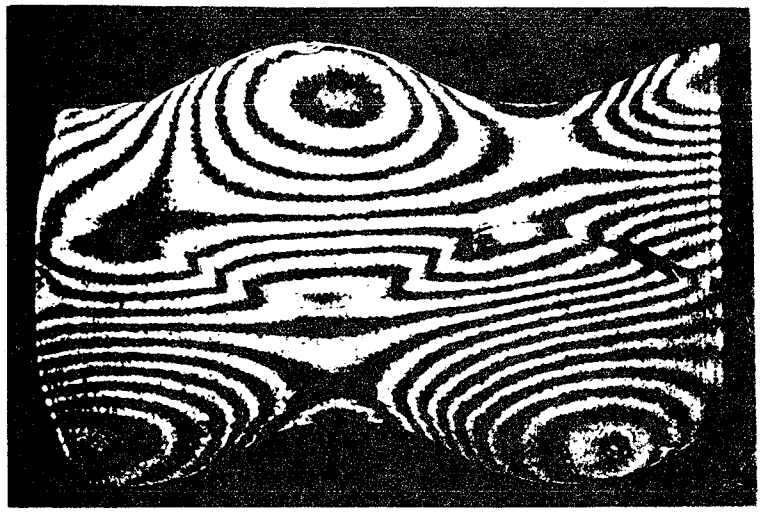

(b)

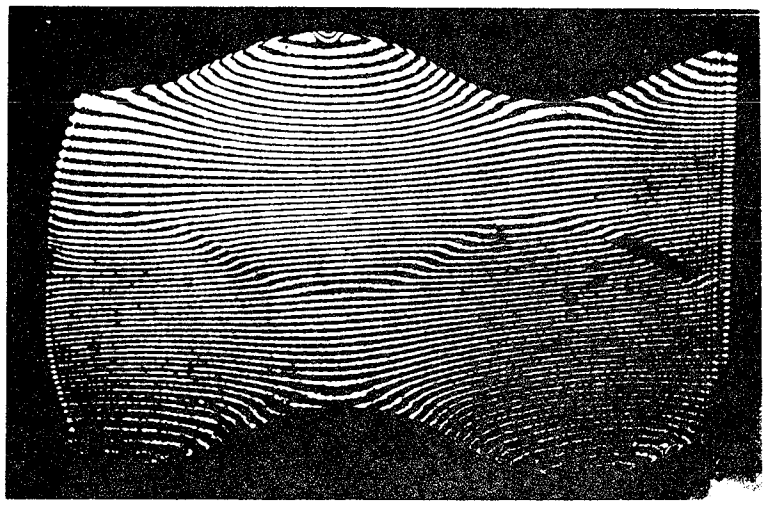

Fig. 27 Transverse Fringe Patterns from an Out-of-Phase Specimen

(a) 150 lb(Nulled-Out)
(b) 150 lb(with Carrier Fringes)
(c) 100 lb

Continued to Next Page

(c)

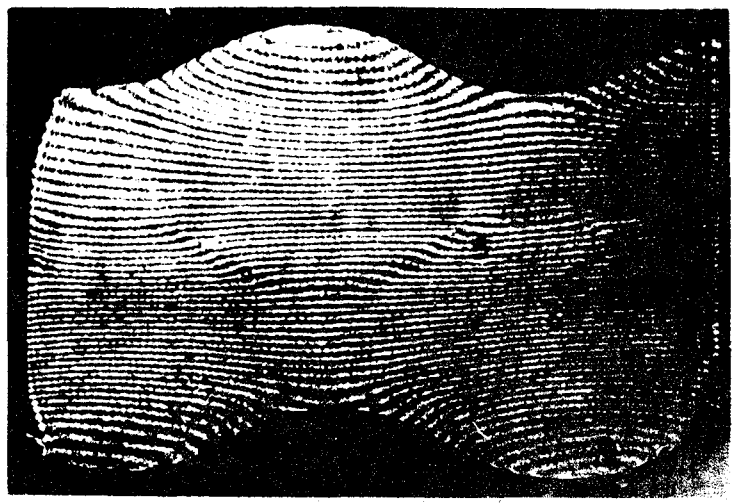

Fig. 27 (Continued)

RESULTS AND DISCUSSION

TENSION TEST

The replicate tension tests for all specimen configurations exhibited fundamentally identical elastic behavior which was remarkably linear and reproducible. From the elastic constants obtained from straight specimens of aluminum and epoxy, the effective non-dimensional Young's modulus was predicted for each specimen configuration. In Fig. 28, the comparisons between the model predictions and the experimental data from the corrugated aluminum specimens are shown for three different thicknesses of the aluminum layers. Experimental data from the two In-Phase and two Out-of-Phase laminate configurations are compared with the model predictions in Fig. 29 and Fig. 30, respectively. The comparisons between the model predictions and experimental data are in good agreement.

As expected from the model, the measured strains were always greater than the actual strains at the neutral axis of the corrugated layers which, in this study, were assumed to be the main load-carrying layers. The pseudo strain computed from the model together with the average of the actual strain over the wave pattern gave a reasonable value to which the measured strain could be directly compared. This is explained by the fact that the contribution of bending strain component cancels out when the indicated strain is measured by an extensometer over one representative pitch of the wavy patterns.

The measured indicated strains of the Out-of-Phase specimens were always slightly greater than the model predictions. One possible explanation for this is that the Out-of-Phase specimen does not exactly

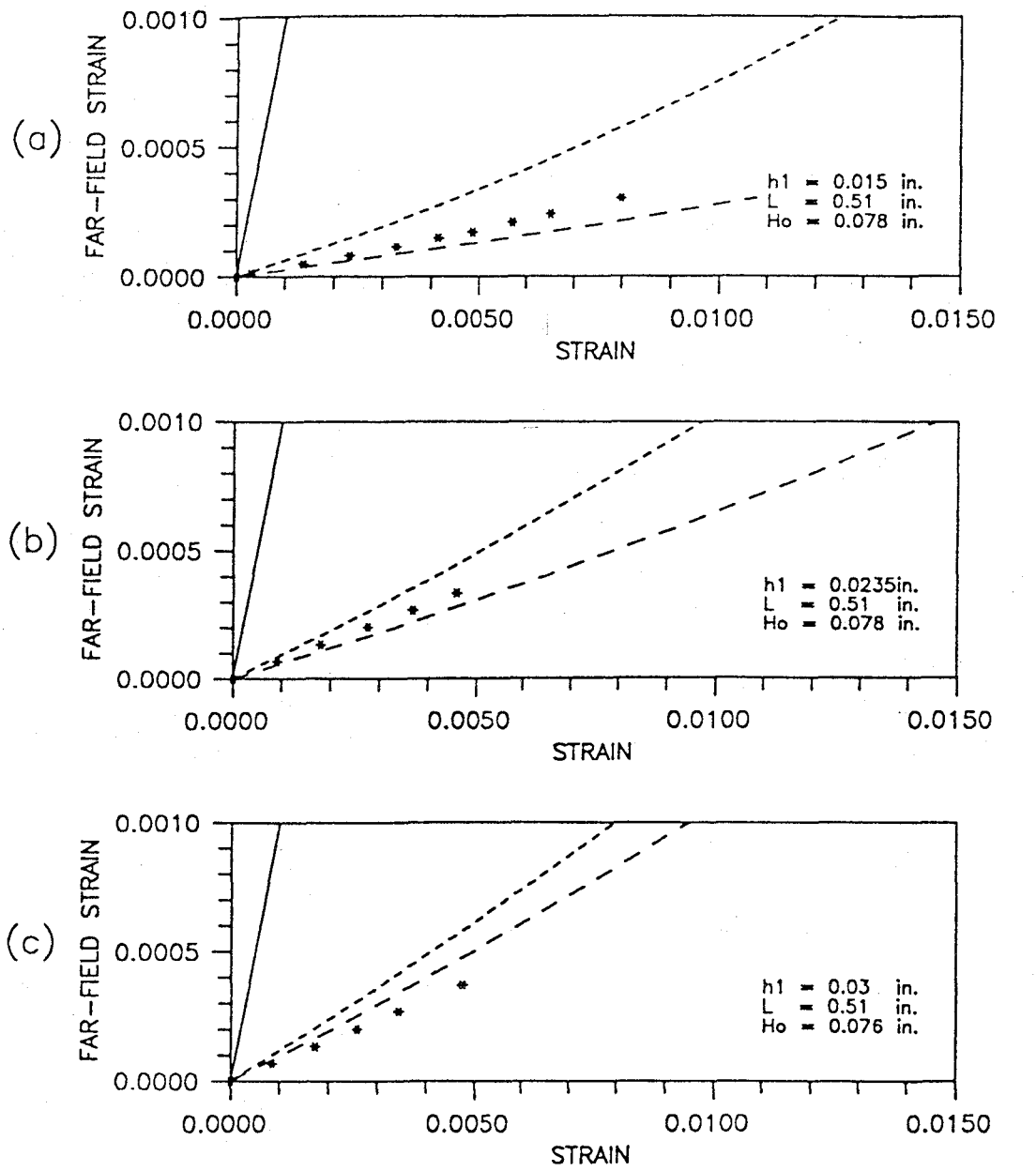

Fig. 28 Comparison between the Model Prediction and Data from Corrugated Aluminum Layers

(a) t = 0.030 inch
(b) t = 0.047 inch
(c) t = 0.060 inch

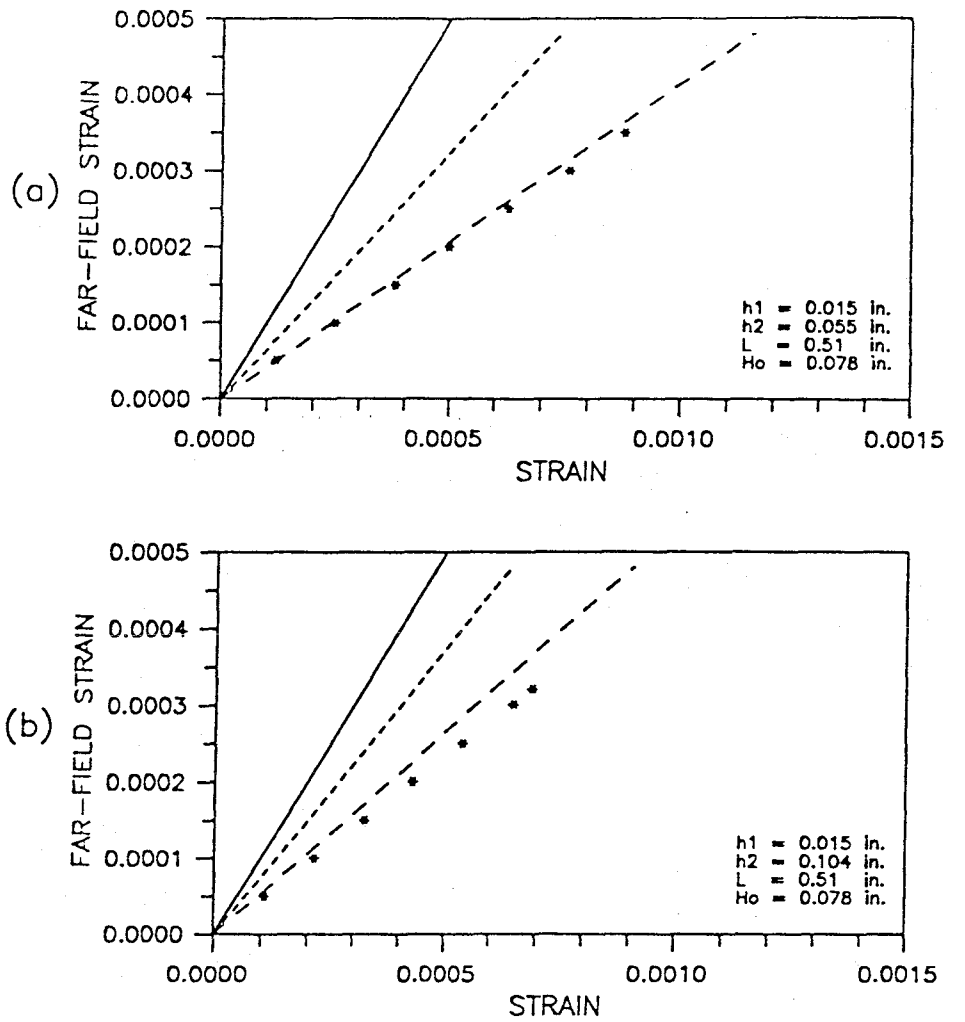

—— FAR-FIELD STRAIN
--- MAX. VALUE OF ACTUAL STRAIN
— — AVE. VALUE OF INDICATED STRAIN
*** EXPERIMENTAL DATA

Fig. 29 Comparison between the Model Prediction and Data from In-Phase Specimens

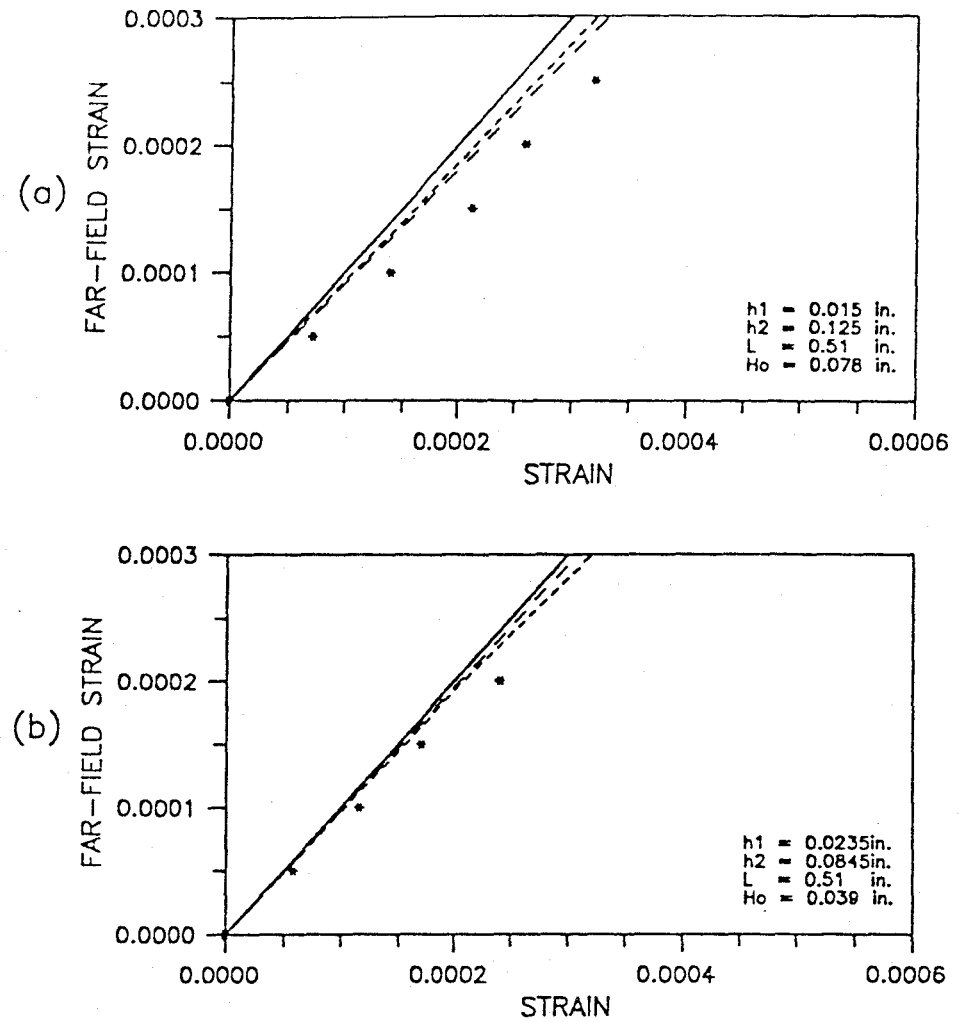

—— FAR-FIELD STRAIN
--- MAX. VALUE OF ACTUAL STRAIN
— — AVE. VALUE OF INDICATED STRAIN
*** EXPERIMENTAL DATA

Fig. 30 Comparison between the Model Prediction and Data from Out-of-Phase Specimens

match the idealized geometries required by the model. The Out-of-Phase specimens tested during this study consist of three aluminum layers resulting in indicated In-Phase patterns between the two outer aluminum layers. The indicated In-Phase bending due to the limited number of aluminum layers may cause additional pseudo strain. However, the In-Phase specimens always satisfy the idealized geometry for one representative segment as required by the model.

The effect of the thickness of the epoxy layer is best illustrated in Fig. 29. As the thickness of the epoxy layer in the In-Phase laminate increases, the difference between the maximum value of predicted actual strain at X = L/2 (ϵ_{ACT}) and the measurable strain ($\epsilon_{IND,AVE}$) decreases. The experimental data obtained from two In-Phase wavy laminate configurations showed the same trend as predicted. The model predictions and measured data from two different Out-of-Phase specimens are also illustrated in Fig. 30. The shifting of the experimental data from ϵ_{ACT} to $\epsilon_{IND,AVE}$ is primarily attributed to the influence of the stretching of the wavy patterns in the main load-carrying layers. This change of the wavy patterns is indicated as if it were real strain due to the limitation of the strain gage length. If the strain gage or extensometer gage length is much smaller than the pitch of the wavy pattern in a laminate, then the actual strain may be directly measurable. However, in most composite laminates containing wavy patterns or wrinkled fibers in the main load-carrying layers including the specimens of this study, the strain gage length has the same order of magnitude as the pitch length of wavy patterns of the layers or wrinkled fibers. Thus, the average value of the pseudo strain (ϵ_{PS}) over one representative segment derived by the model should be taken into con-

sideration to predict the effective Young's moduli of composite materials with wavy layers or wrinkled fibers.

MOIRE TEST

Moire fringe patterns taken from In-Phase and Out-of-Phase specimens were shown in Fig. 23-27. As previously discussed, the fringe patterns were enhanced by the addition of initial carrier fringe patterns, instead of null field fringe patterns. Therefore, only the differences in bending strain components between the upper and lower surfaces of the aluminum layers were calculated and are compared with the model predictions for both In-Phase and Out-of-Phase specimens in Fig. 31-32. For more details of the fringe pattern analysis, please refer to the Appendix.

The transverse fringe patterns from In-Phase and Out-of-Phase specimens confirmed the main assumption of the model. Comparing Figs. 24-d and 27-a, it is obvious that the fringe patterns for the two specimen configurations are fundamentally different. The rotation of the fringes illustrated in Fig. 24-d is characteristic of shear deformation. Furthermore, the number of fringes through the thickness is relatively constant. The bull's eye pattern illustrated in Fig. 27-a is characteristic of tension-compression behavior. Also, the number of fringes through the thickness varies along the axial direction of the Out-of-Phase specimen. This provides qualitative confirmation that the matrix layers of the In-Phase specimen is shear dominated while the matrix layers of the Out-of-Phase specimen is governed by tension-compression behavior.

The pseudo strain components could not be compared with the model

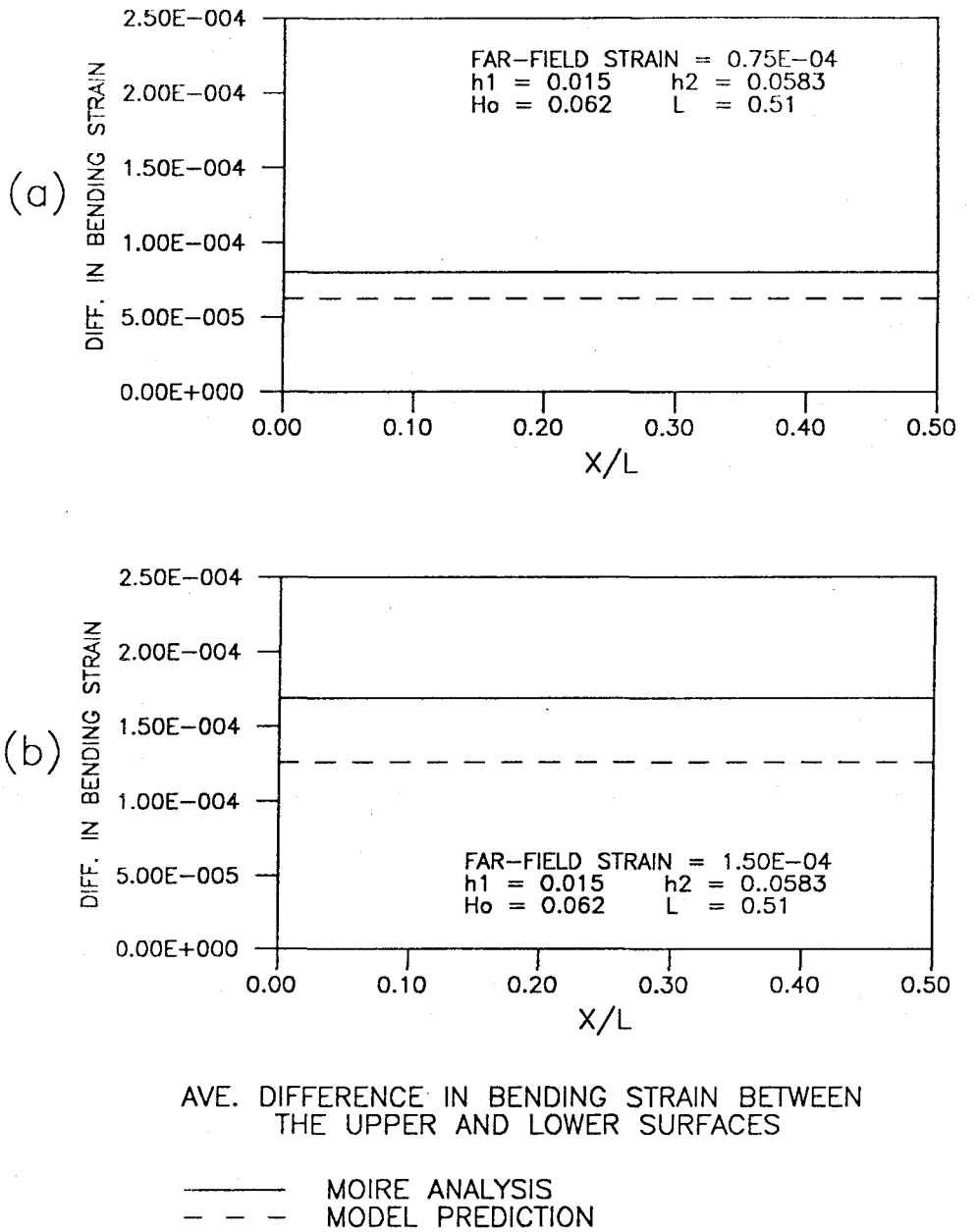

Fig. 31 Average Difference in Bending Strain between the Upper and Lower Surfaces of the In-Phase Specimen

(a) 80 lb Tension
(b) 160 lb Tension

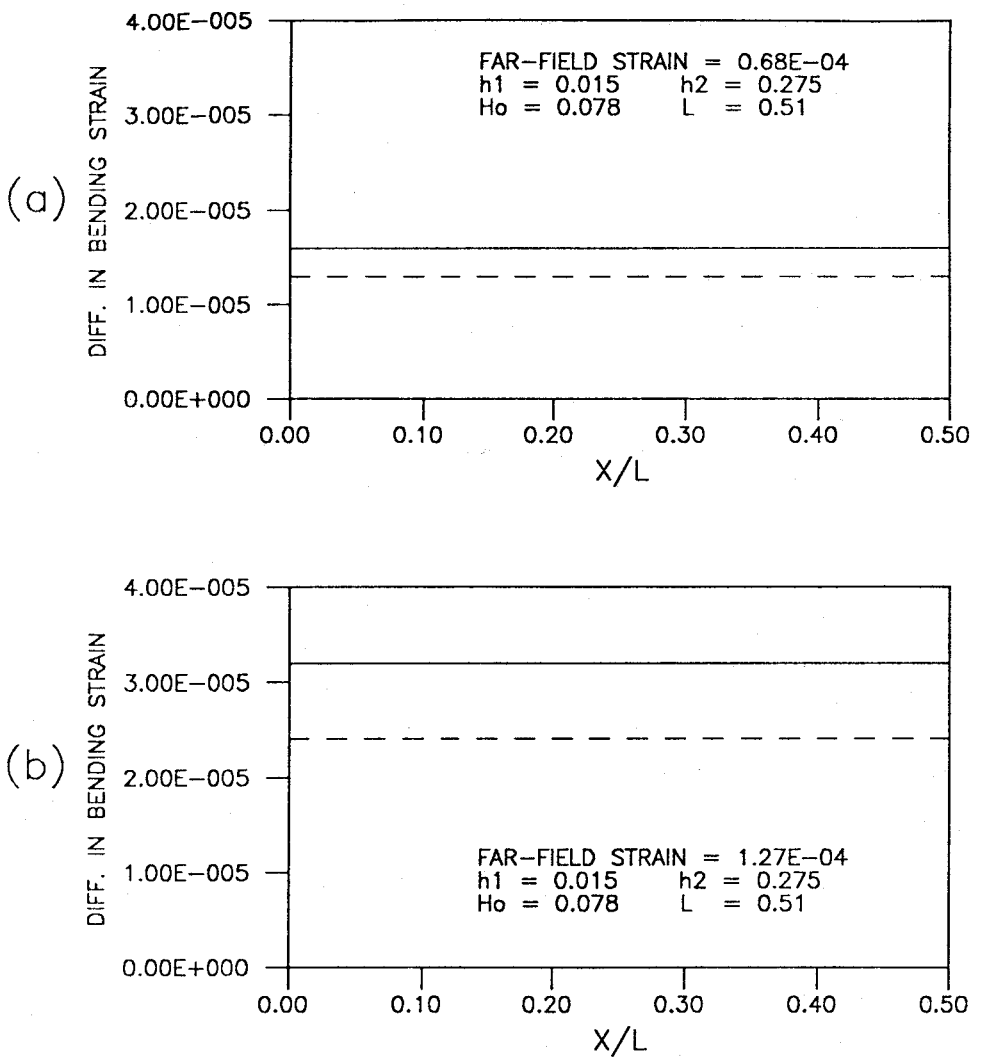

Fig. 32 Average Difference in Bending Strain between the Upper and Lower Surfaces of the Out-of-Phase Specimen

(a) 80 lb Tension
(b) 150 lb Tension

predictions because the rigid body rotations of the hinge mechanism used for the specimen installation were coupled to the axial and transverse deformation of the specimens. This coupling effect changed the number of fringes in the axial displacement field as well as the transverse displacement field. However, these rigid body rotations due to the hinge mechanism may be eliminated by calculating the difference in the number of fringes between the upper and lower surfaces of the center aluminum layers as illustrated in Figs. 33 and 34. The difference in the number of fringes between the upper and lower surfaces are the same in both figures. Both figures are taken from one specimen under the same loading condition, 67.5kg(150lb) in tension, but with different initial carrier fringe patterns.

The variation of the pseudo strain along the curvature in the In-Phase specimen can be qualitatively checked from Fig. 35. Exact numerical data for the pseudo strain and far-field strain could not be retrieved from the moire fringe analysis because of the rigid body rotation problem. The general trend of the pseudo strain obtained from the In-Phase specimen shows a good agreement with that from the model prediction as illustrated in Fig. 35 confirming that the pseudo strain component is a cosine function of the x. This variation of the pseudo strain component along the x axis does not give a practical effect on the effective Young's modulus of a wavy specimen. This is because the strain measuring device accesses only the average value of the sum of the pseudo strain and constant axial strain along the neutral axis of the wavy layer when the gage length is equal to or longer than one representative pitch of the wavy pattern.

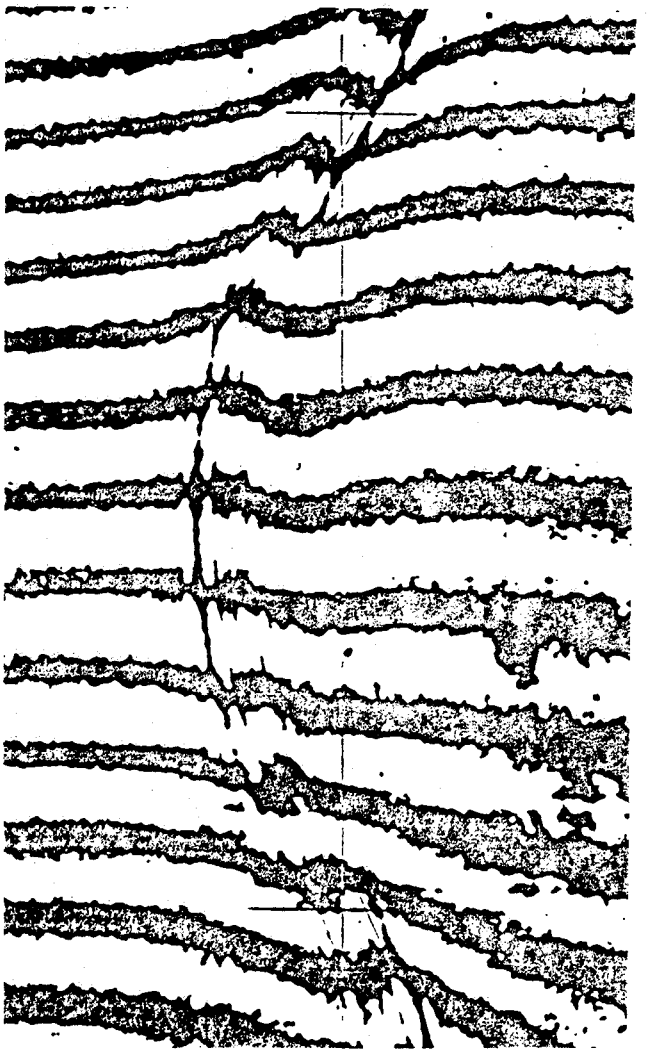

Fig. 33 Moire Pattern with Less Carrier Fringes

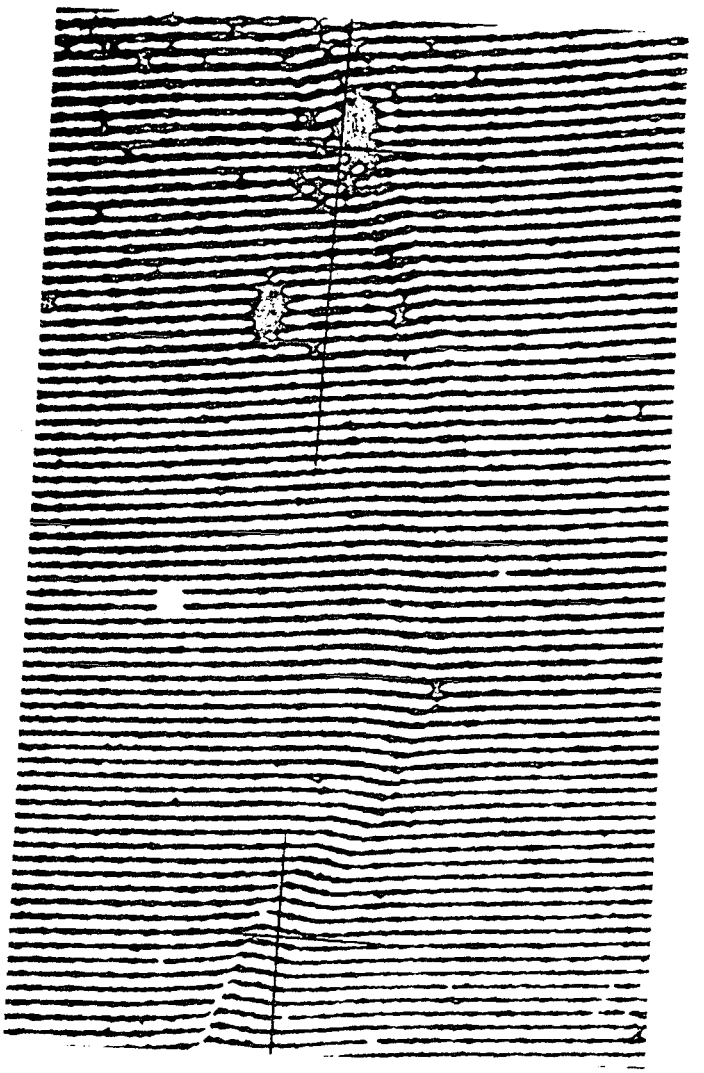

Fig. 34 Moire Pattern with More Carrier Fringes

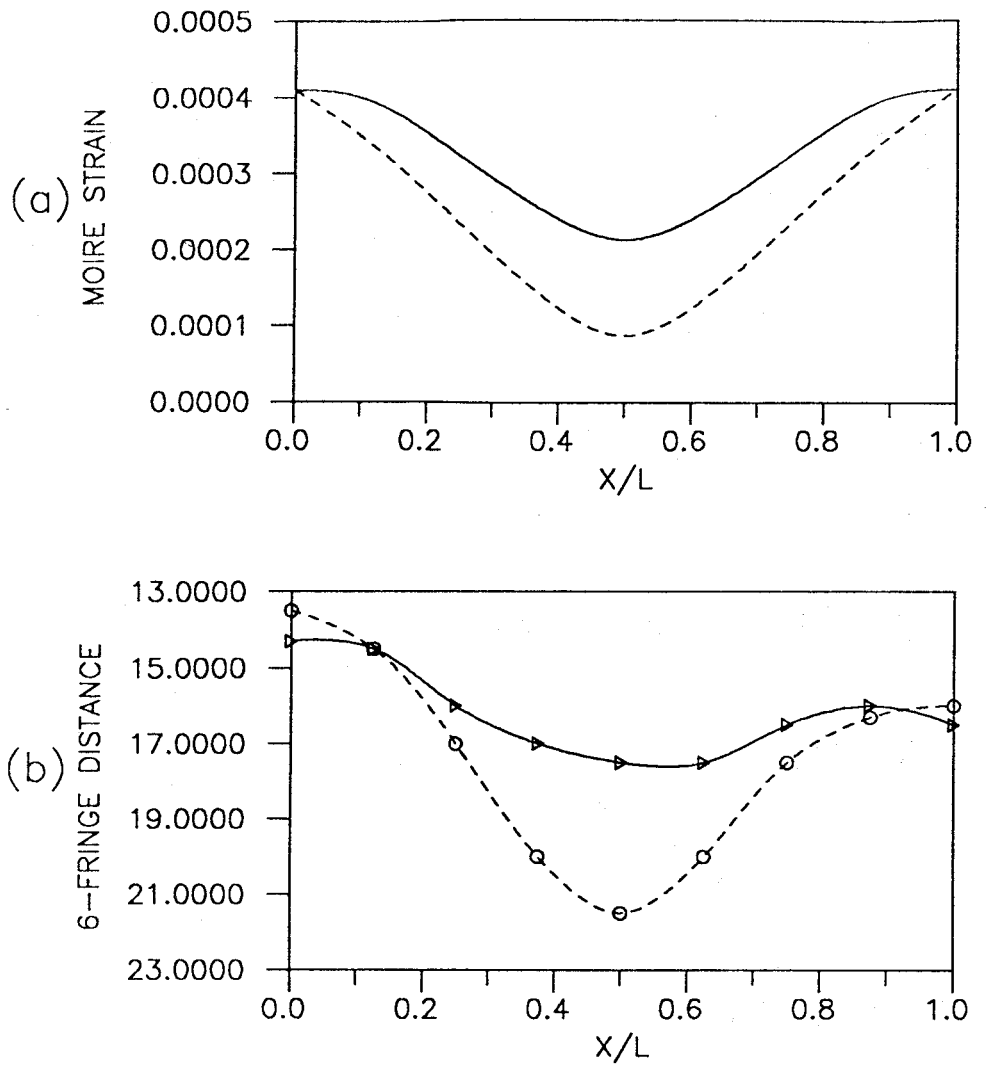

Fig. 35 Variation of the Total Strain in the In-Phase Specimen (Refer to Appendix)

(a) Model Prediction
(b) Moire Analysis

APPLICATIONS OF THE MODEL

THE MODEL PREDICTIONS AND OTHER EXPERIMENTS

By applying a maximum strain failure criterion to the wavy layer, analytical results from the mathematical models may be used to predict the strength of composites with in-situ local curvature in the reinforcement. For an In-Phase laminate, eq. (11) and eq. (21) can be rewritten as:

$$\epsilon_{YLD} \geq \epsilon_o \left\{ 1 + \frac{\pi^2 (H_o h_1 / L^2)}{\epsilon_o + \dfrac{h_2^2 \, G_{XZ}/E}{h_1(h_2 - h_1)} + \dfrac{\pi^2}{3}(h_1/L)^2} \right\} \qquad (36\text{-}1)$$

Neglecting the first term and the last term of the denominator in eq. (36-1) and rearranging gives the critical far-field strain:

$$\epsilon_{cr} \leq \epsilon_{YLD} \left\{ \frac{1}{1 + \pi^2 (H_o h_1 / L^2)[h_1(h_2 - h_1)/h_2^2](E/G_{XZ})} \right\} \qquad (36\text{-}2)$$

In this section, experimental results reported by other experimentalists[1-3] are compared with the model predictions. Those experimental studies were selected by the author for the following reasons.

1. The experimental result reported by Poe[1] contains an exact numerical value of strength reduction as the result of wavy patterns in a specimen configuration. Also, one of Poe's specimens was available to measure the geometrical parameters.

2. The stitched composites studied by Dexter[2] contained repeated

wavy pattern with accurate pitches. Other geometrical parameters were measurable from his paper.

3. The geometrical parameters of the helical tungsten fibers for a metal matrix composite and the stress-strain curve of the helical fibers were compared with those of straight tungsten fibers in the experimental study conducted by Kagawa[3].

In order to compare the model predictions with other experimental data, the material properties of the main load-carrying layers and the geometrical parameters are required as input data for the model. The three experimental studies mentioned above include this information. The material properties and geometrical parameters related to these experimental studies and comparison with the present model predictions are given Table 4 and Fig. 36. The ultimate strength for Poe[1] and Dexter[2] were calculated from the ultimate tensile strain under the assumption that the specimen will fail if the outermost fiber at the concave side of the wavy layer reaches its ultimate strain measured from an equivalent straight fiber or layer. The comparison of the model prediction with Poe's experiment[1] is not as good as with Dexter[2] as shown in Table 4. Also, the In-Phase model gives better results than the Out-of-phase model for comparing with both experimental results.

In Fig. 36, the present model may be used to predict the effective young modulus and the local yield point of Kagawa's helical fibers[3]. Kagawa's stress-strain curve shows a very interesting change in the effective Young's modulus which is almost linear before and after the local yield point. One possible explanation is the fact that, under certain geometries, the local plastic zone will gradually propagate from the concave surface to the convex surface and also from the maxi-

Table 4. Applications to "REAL" Composites

Author	Ref.	Reported Strength Reduction	Parameters	Analytical Prediction	
				In-Phase	Out-of-Phase
Poe	[1]	39 %	$E_f/E_m = 20$ $E_f/G_m = 40$ L=20, h1=1 h2=5, Ho=2	23 %	5 %
Dexter & Funk	[2]	25 %	$E_f/E_m = 20$ $E_f/G_m = 40$ L=20, h1=2 h2=6, Ho=1	25 %	14 %

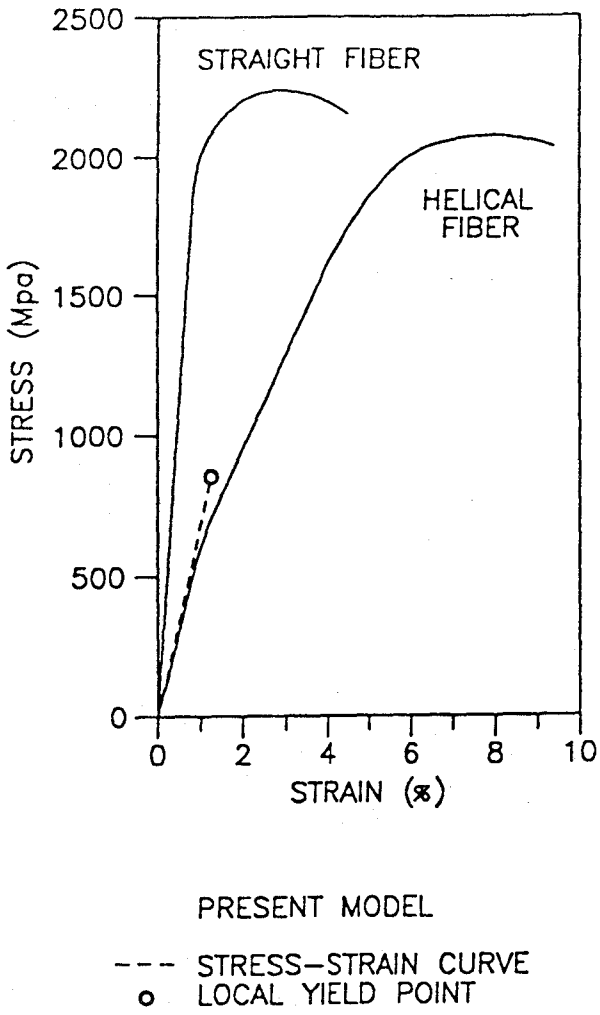

Fig. 36 Comparison with Kagawa's Experiment[3]

mum rising point to the inflection point of the wavy pattern. Then the effective Young's modulus will decrease after the local yield point is reached and exhibit almost linear elastic behavior until the elastic deformation and plastic deformation equilibriate each other. Once this equilibrium point is reached, the plastic zone will stop propagating to the adjacent material which is within the elastic range. Thereafter, increasing the tension load will result in failure of the plastically deformed region much like a straight specimen failure after its yield point is exceeded.

COMPARISON WITH OTHER MODELS

Some of the mathematical models given in the literature [8 and 13] are actually special cases of the present model. Also these studies [8 and 13] do not include the shear term given in eq. (7). The governing differential equation of the blister model[13] is a special case of the Out-of-Phase governing differential equation given by eq. (32). Also, the equivalent spring constant in ref.[13] is a special case of the linear spring constant given by eq. (30).

$$D\frac{d^4w_2}{dx^4} + P_1\frac{d^2w_2}{dx^2} + kw_2 = 0 \qquad (37)$$

where

$$k = E_r/t_r$$

The tie-bar/column model[8] assumed an infinite matrix material and its governing equation is that of the Out-of-Phase case, but the elas-

tic constraint due to an infinite matrix material cannot be calculated from the present model.

$$E_f I\frac{d^4w}{dx^4} - F\frac{d^2w}{dx^2} + kw = F\frac{d^2w_o}{dx^2} \tag{38}$$

where

$$k = \frac{16\pi G_m}{1+6(1-2\upsilon_m)} \tag{39}$$

Using the same input data(Table 5) given in Jortner's numerical investigation[9], a similar result is obtained by the present model. The comparison is shown in Fig. 37.

Equation (7) is easily modified to the governing differential equation of the shear mode buckling of a composite without initial curvature in the main load-carrying layers or in the reinforcing fibers.

$$EI\frac{d^4w}{dx^4} + (K_M+P)\frac{d^2w}{dx^2} = 0 \tag{40}$$

Let $w = a_1\sin(m\pi x/L)$. Then, substituting w into eq. (40) gives

$$[EI(m\pi/L)^4 - (K_M+P)(m\pi/L)^2]a_1\sin(m\pi x/L) = 0 \tag{41}$$

$$-K_M = \alpha^2 K_T = [h_2/(h_2-h_1)]^2 K_T = [2h_2^2/(h_2-h_1)]G_m \tag{42}$$

Table 5. Jortner's Ideal Material
Given in Ref.[9]

Case Name	E_a	E_b	E_c	ν_{bc}	ν_{ac}	ν_{ab}	G_{bc}	G_{ac}	G_{ab}
Base Line	12.0	2.0	12.0	0.0	0.0	0.1	1.0	1.0	1.0
High G_{ab}	12.0	2.0	12.0	0.0	0.0	0.1	1.0	1.0	2.0
Low G_{ab}	12.0	2.0	12.0	0.0	0.0	0.1	1.0	1.0	0.1
High E_b	12.0	12.0	12.0	0.0	0.0	0.1	1.0	1.0	1.0

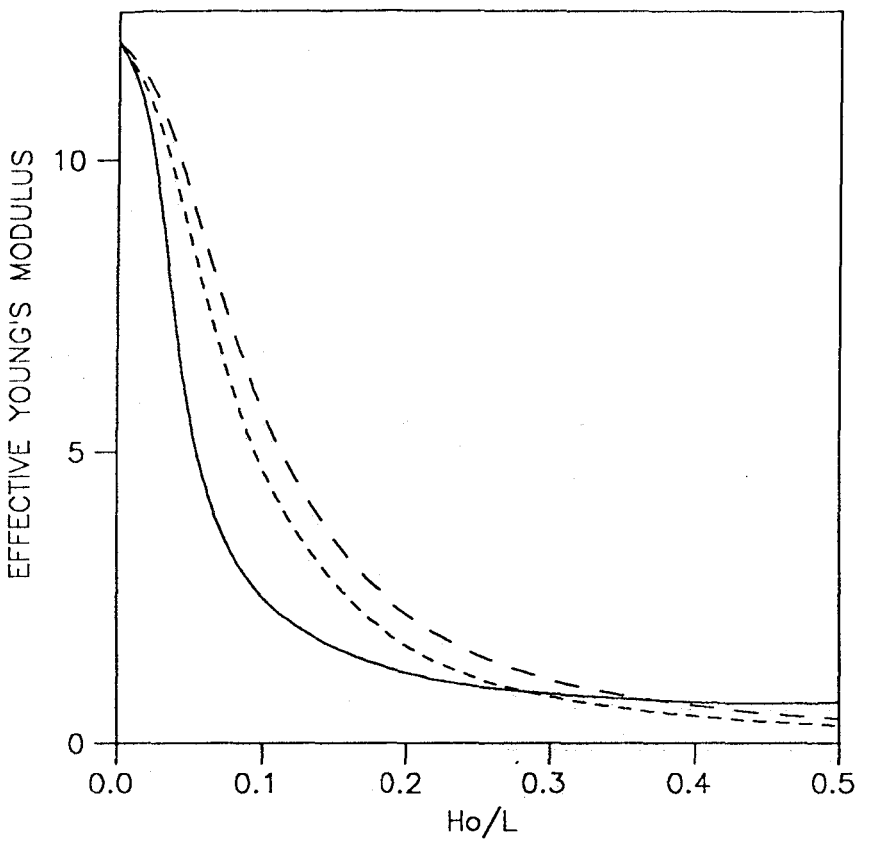

Fig. 37 Comparison with Jortner's Result[9]

Then the critical load for buckling is given by

$$P_{cr} = 2h_1\epsilon_o E_f = 2h_1\sigma_f$$

$$= EIm^2\pi^2/L^2 + [(2h_2^2/(h_2-h_1)]G_m \tag{43}$$

Note that $I=2h_1^3/3$, $h_2/h_1 = 1/v_f$, and $h_2/(h_2-h_1) = 1/(1-v_f)$.

Then,

$$\sigma_f = \frac{E\pi^2}{3}(mh_1/L)^2 + \frac{G_m}{v_f(1-v_f)} \tag{44}$$

Assuming that $mh_1/L<<1$, then

$$\sigma_f = \frac{G_m}{v_f(1-v_f)} \tag{45}$$

The far-field stress is given by

$$\sigma_{cr} = v_f\sigma_f + (1-v_f)\sigma_m \simeq v_f\sigma_f \tag{46}$$

Therefore, the critical far-field stress for buckling is given by

$$\sigma_{cr} = \frac{G_m}{(1-v_f)} \tag{47}$$

This result is identical to Rosen's result[7].

If the shear deformation of the fiber reinforcement is taken into account, then Rosen's shear mode buckling model becomes the shear instability failure model proposed by Hayashi[16] given as

$$\sigma_{cr} = \frac{G_m}{v_f \frac{G_m}{G_f} + (1-v_f)} \tag{48}$$

Lager and June[17] modified Rosen's model for their experimental study by including an influence factor as

$$\sigma_{cr} = \frac{0.63 G_m}{1-v_f} \tag{49}$$

It is obvious that eq. (47) and eq. (49) cannot be used for predicting the critical stress for the shear mode buckling of a composite with a high fiber volume fraction. The difference between eq. (47) and eq. (48) is caused by the difference in the assumptions for the elastic constraint on the reinforcement, i.e., the present model assumes the shear strain of the fiber to be neglected, while Hayashi's model assumes the shear stress to be constant in the fiber and the matrix.

CONCLUSIONS

A mathematical model based on the Euler-Bernoulli beam theory is proposed for predicting the influence of wavy patterns in the main load-carrying layers or wrinkled fibers on the laminate behavior under tensile loading. The main load-carrying layers or wrinkled fibers were assumed to be corrugated beams embedded in elastic foundations of various spring constants. The effective Young's moduli of different laminate configurations were experimentally determined and compared to the predicted values computed from the model. The bending strains in the wavy layers were also predicted by the model and compared with the experimental results from moire fringe analysis.

The model predictions were in close agreement with the present experimental results including both extensometer measurements and moire interferometry fringe pattern analysis. Furthermore, experimental results reported by other researchers were compared with the present model showing good agreement. From the comparison between the model and experimental results, the following conclusions were obtained:

1. The model proposed in this study gives an accurate prediction of the effective Young's modulus of a laminate containing wavy layers and the actual strain in the main load-carrying layer in a wavy laminate of different wavy patterns.

2. The pseudo strain due to the change of the geometry of the wavy layers must be taken into consideration for computing the effective Young's modulus even for very small amplitude wavy patterns.

3. The model can be applicable for determining the effective Young's moduli and ultimate strengths of in-situ laminated composites

containing wavy patterns under tension loading in the direction of the wavy patterns.

The present model has three disadvantages. First, it does not give the interfacial stresses between the main load-carrying layers and the matrix layers because the stress and deformation of the matrix layers are assumed to be constant through the thickness. Therefore, failure modes such as delamination cannot be addressed. By combining the present model and the approach of Akbarov & Guz [10,11], the interfacial stress components in a wavy laminate can be calculated. Second, the model is not directly applicable to anisotropic materials containing wavy layers. To extend the present model to anisotropic materials, the model must be generalized in a way similar to the mathematical model proposed by Shuart[14]. Finally, the stress-strain state in the matrix material cannot be accurately predicted by the model. This is because the deformation behavior of the matrix material was idealized as simple uniform shear or tension-compression, which was only qualitatively confirmed by the moire analysis.

In conclusion, the model generated herein gives a reasonable first approximation of the effective Young's modulus of composites containing local curvature in the reinforcement. Furthermore, while the strength issue has not been fully investigated, the model appears to give a reasonable approximation of the failure of the reinforcing layer.

REFERENCES

1. Poe, C. C., Jr., Illg, W., and Garber, D. P., "Tension Strength of a Thick Graphite/Epoxy Laminate after Impact by a 1/2-in.-radius Impactor," NASA TM-87771 National Aeronautics and Space Administration, Washington, D.C., July 1986.

2. Dexter, H. B. and Funk, J. G., "Impact Resistance and Interlamina Fracture Toughness of Through-the-Thickness reinforced Graphite/Epoxy," AIAA Paper 86-1020-CP, May 1986.

3. Kagawa, Y., Nakata, E., and Yoshida, S., "Fracture Behavior and Toughness of Helical Fiber Reinforced Composite Metals," Proceedings of the 4th International Conference on Composite materials, ICCN-IV, October 1982.

4. Makarov, B. P. and Nikolaev, V. P., "Effect of Curvature of the Reinforcement on the Mechanical and Thermophysical Properties of a Composite," Polymer Mechanics(Translated from Russian), No.6, November-December,1971.

5. Simonds, R. A., Stinchcomb, W., and Jones, R. M., "Mechanical Behavior of Braided Composite Materials," Composite Materials: Testing and Design(8th Conference), ASTM STP 972, J. D. Whitcomb, Ed., American Society for Testing and Materials, Philadelphia, April 29-May 1, 1986.

6. Davis, J. G., Jr., "Compressive Strength of Fiber-Reinforced Composite Materials," Composite Reliability, ASTM STP 580, American Society for Testing and Materials, Philadelphia, pp.364-377, 1975.

7. Rosen, B. W., "Mechanics of Composite Strengthening," Fiber Composite Materials, American Society for Metals, pp.37-75, 1965.

8. Bert, C. W., "Micromechanics of the Different Elastic Behavior of Filamentary Composites in Tension and Compression," Mechanics of Bimodulus Materials, ASME, New York, AMD-Vol. 33, pp.17-28, December, 1979.

9. Jortner, J., "A Model for Predicting Thermal and Elastic Constants of Wrinkled Regions in Composite Materials," Effects of Defects in Composite Materials, ASTM STP 836, American Society for Testing and Materials, Philadelphia, pp.217-236, 1984.

10. Akbarov, S. D. and Guz, A. N., "Stressed State in a Composite Materials with Curved Layers Having a Low Filler Concentration, " Mechanics of Composite Materials (Translated from Russian), Consultant Bureau, New York, pp.688-693, May 1985, (Russian Original, Vol. 20, No.6, 1984).

11. Akbarov, S. D. and Guz, A. N., "Model of a Piecewise Homogeneous body in the Mechanics of Laminar Composites with Fine-Scale curvatures," Soviet Applied Mechanics (Translated from Russian), Consultant Bureau, New York, pp.313-319, October 1985, (Russian Original, Vol. 21, No.4, 1985.)

12. Ishikawa, T., Matsushima, M., Hayashi, Y., and Chow, T., "Experimental Confirmation of the Theory of Elastic Moduli of Fabric Composites," Journal of Composite Materials, Vol. 19, pp.443-458, September 1985.

13. El-Senussi, A. K. and Webber, J. P. H, "Blister Delamination Analysis Using Beam-Column Theory with an Energy Release Rate Criterion," Composite Structures, Vol. 5, pp.125-142, 1986.

14. Shuart, M. J., "Short-Wavelength Buckling and Shear Failure for Compression-Loaded Composite Materials," NASA TM 87640, National Aeronautics and Space Administration, Washington, D.C., November, 1985.

15. Post, D., "Moire Interferometry," SESA Handbook on Experimental Mechanics, Albert S. Kobayashi, Ed., 1987.

16. Hayashi, T., " On the Shear Instability of Structures Caused by Compressive Load," AIAA Paper No. 65-770, 1965.

17. Lager, J. B. and June, R. R., "Compressive Strength of Boron-Epoxy Composites," Journal of Composite Materials, vol. 3, No. 1, pp.48-56, 1969.

18. Shames, I. H. and Dym C. L., Energy and Finite Element Methods in Structural Mechanics, McGraw-Hill, pp.424, 1985.

19. Timoshenko, S. P. and Gere, J. M., Theory of Elastic Stability, McGraw-Hill, Second Edition, pp.32, 1983.

APPENDIX (EXAMPLE OF THE MOIRE FRINGE ANALYSIS)

The displacement and strain relationships to calculate strains from a moire fringe pattern can be expressed by the following equations:

$$\Delta U_x = \Delta N_x / f$$

$$\Delta U_y = \Delta N_y / f$$

$$\epsilon_{xx} = \Delta U_x / \Delta x$$

$$\epsilon_{yy} = \Delta U_y / \Delta y$$

$$\epsilon_{xy} = \Delta U_x / \Delta y + \Delta U_y / \Delta x$$

Where

ΔN_x = the increment of the number of fringes in the x direction.

ΔN_y = the increment of the number of fringes in the y direction.

f = frequency of the moire grating for the present study
= 2400 lines/mm (60960 lines/in.)

To obtain the difference in the bending strain component from Fig. 38, the number of fringes between two inflection points of the curvature must be counted. In Fig. 38-(a), the initial difference in the number of fringes between the upper and lower surfaces of the aluminum layer is 0.25. Likewise, in Figs. 38-(b) and (c), the differences are -0.25 and -0.75, respectively. Compensating for the initial difference at the zero loading condition gives

ΔN_x = 0 at the zero loading condition

ΔN_x = -0.5 at 80 lb. tension

ΔN_x = -1.0 at 160 lb. tension

Since the distance between the two inflection points is 0.51 in., half of the curvature pitch, the average difference in the bending strain component between the upper and lower surfaces, ϵ_{diff}, for each loading condition is given by

ϵ_{diff} = 0

ϵ_{diff} = 0.5÷60960÷0.51 = 1.61 E-5 at 80 lb. tension,

and

ϵ_{diff} = 1÷60960÷0.51 = 3.22 E-5 at 160 lb. tension.

These strain values are compared with the model predictions in Fig. 32.

To check the total strain variation along the upper and lower surfaces of the main load-carrying layer, the moire fringe pattern illustrated in Fig. 39 was analyzed for the In-Phase specimen under 160 lb. tension. Due to the unknown increment of the fringes caused by rigid body rotations of the specimen during loading, the numerical strain value cannot be calculated from the fringe pattern. But the general trend of the total strain variation along the upper and lower surfaces are in good agreement to the model prediction as shown in Fig. 35.

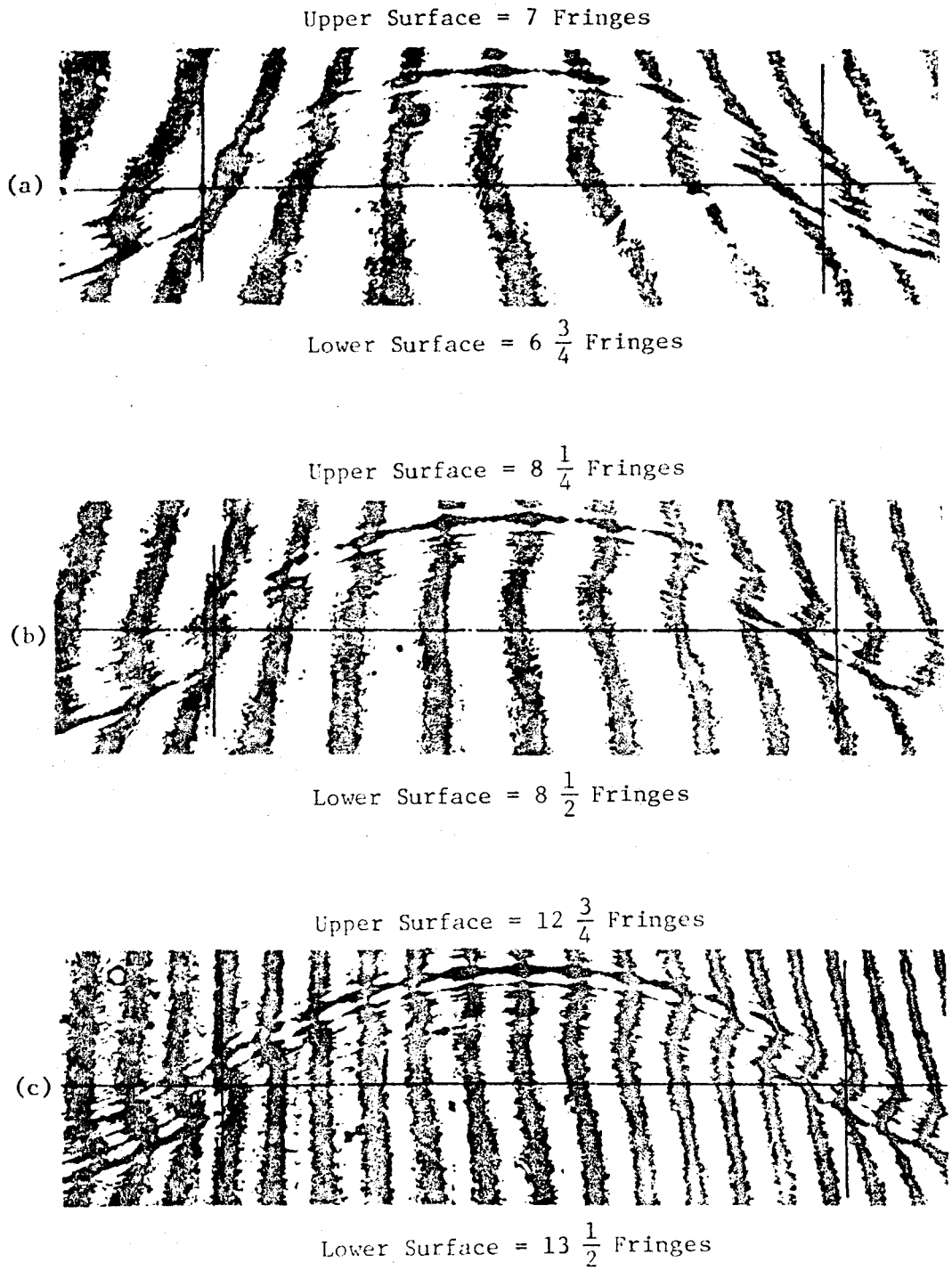

Fig. 38 Change of Fringe Pattern in the Out-of-Phase Specimen

(a) 0 lb Tension
(b) 80 lb Tension
(c) 150 lb Tension

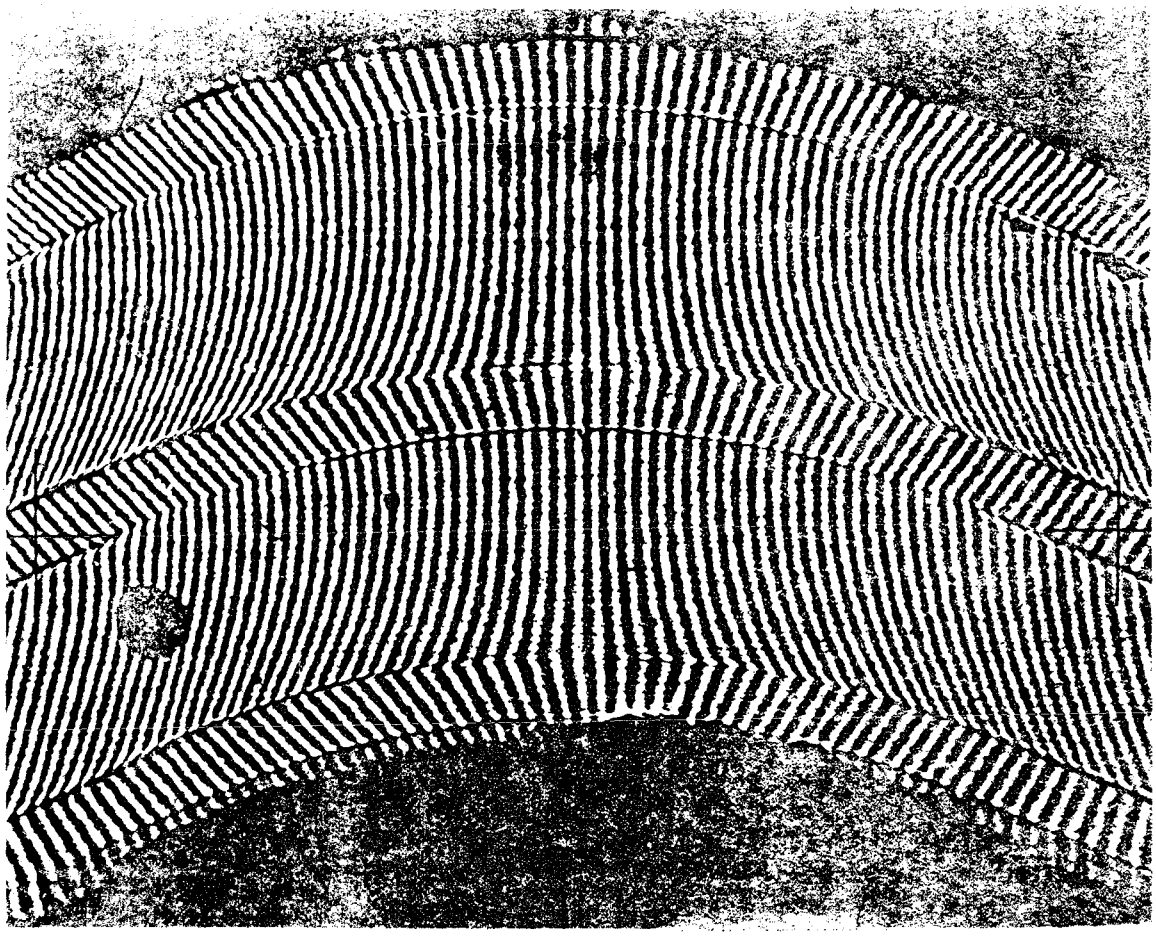

Fig. 39 Sample Fringe Pattern for Analyzing the Total Strain Variation (In-Phase)

NASA

Report Documentation Page

1. Report No.	2. Government Accession No.	3. Recipient's Catalog No.
NASA CR-181670		

4. Title and Subtitle
A MICROMECHANICS MODEL OF THE STIFFNESS AND STRENGTH OF LAMINATES WITH FIBER WAVINESS

5. Report Date
July 1988

6. Performing Organization Code

7. Author(s)
Charles E. Harris and Jong-Won Lee

8. Performing Organization Report No.

10. Work Unit No.
506-43-11-04

9. Performing Organization Name and Address
Texas A&M University
Aerospace Engineering Department
College Station, TX 77841

11. Contract or Grant No.
NAG1-711

13. Type of Report and Period Covered
Contractor Report

12. Sponsoring Agency Name and Address
National Aeronautics and Space Administration
Langley Research Center
Hampton, VA 23665-5225

14. Sponsoring Agency Code

15. Supplementary Notes
Langley Technical Monitor: C. C. Poe, Jr.

16. Abstract
A mathematical model based on the Euler-Bernoulli beam theory is proposed for predicting the effective Young's moduli of piecewise isotropic composite laminates with local ply curvatures in the main load-carrying layers. Strains in corrugated layers, In-Phase layers, and Out-of-Phase layers are predicted for various geometries and material configurations by assuming matrix layers as elastic foundations of different spring constants.

The effective Young's moduli measured from corrugated aluminum specimens and aluminum/epoxy specimens with In-Phase and Out-of-Phase wavy patterns coincide very well with the model predictions. Moire fringe analysis of an In-Phase specimen and an Out-of-Phase specimen are also presented confirming the main assumption of the model related to the elastic constraint due to the matrix layers. The present model is also compared with the experimental results and other models, including the micro-buckling models, published in the literature.

The results of the present study show that even a very small-scale local ply curvature produces a noticeable effect on the mechanical constitutive behavior of a laminated composite.

17. Key Words (Suggested by Author(s))

Laminated composites	In-phase
Main load-carrying layer	Out-of-Phase
Wavy pattern	Pseudo strain
Local ply curvature	Tension
Corrugated beam	Compression

18. Distribution Statement
Unclassified - Unlimited
Subject Category - 24

19. Security Classif. (of this report)	20. Security Classif. (of this page)	21. No. of pages	22. Price
Unclassified	Unclassified	101	A06

End of Document